The Abdus Salam
International Centre for Theoretical Physics

United Nations
Educational, Scientific and
Cultural Organization

IAEA
International Atomic Energy Agency

2152-23

Joint ICTP-IAEA Course on Natural Circulation Phenomena and Passive Safety Systems in Advanced Water Cooled Reactors

17 - 21 May 2010

STABILITY ANALYSIS OF NC BASED SYSTEMS: PRESSURE TUBE TYPE BWR AND STEAM GENERATORS

P.K. Vijayan and A.K. Nayak
Reactor Engineering Division
Bhabha Atomic Research Centre Trombay
Mumbai
India

IAEA Training Course on Natural Circulation Phenomena and Passive Safety Systems in Advanced Water-Cooled Reactors, ICTP, Trieste, Italy, 17-21 May 2010

Lecture Notes for T-08

on

STABILITY ANALYSIS OF NC BASED SYSTEMS: PRESSURE TUBE TYPE BWR AND STEAM GENERATORS

by

P.K. Vijayan and A.K. Nayak

Reactor Engineering Division, Bhabha Atomic Research Centre
Trombay, Mumbai-400085, INDIA

May 2010

STABILITY ANALYSIS OF NC BASED SYSTEMS: PRESSURE TUBE TYPE BWR AND STEAM GENERATORS

P.K. Vijayan and A.K. Nayak
Reactor Engineering Division, Bhabha Atomic Research Centre, Trombay, Mumbai 400085, India

1: E-mail: vijayanp@barc.gov.in
2: E-mail: arunths@barc.gov.in

KEY WORDS

Linear stability analysis, Nonlinear stability analysis

LECTURE OBJECTIVES

This lecture reviews the methods used for the analysis of static, dynamic and compound dynamic instabilities in NCSs. The difference between the linear, nonlinear and the need to use both techniques in the stability analysis of NCRs is brought out. Effect of various geometric and operating parameters on the instability is presented taking a pressure tube type reactor as an example. The issues during the start-up of a natural circulation reactor are briefly described.

1. INTRODUCTION

Industrial natural circulation systems must operate stably and reliably over the entire range of power from start-up to full power. To ensure this, we must restrict operation of NCSs well within the stable zone. Thus, there is a need to establish the stable and unstable zones of operation of a NCS. The stable and unstable zones are usually identified by a linear stability (also known as frequency domain) analysis. To have flexibility in operation one also needs to know the effect of various operating parameters like power, pressure, inlet subcooling and design parameters like riser height, inlet orificing and loop geometry on the stability behaviour. Further, in many instances, there is a possibility that NCSs can land in an unstable zone of operation because of a system malfunction, an operator error, or an unanticipated transient. In such cases, the designer must be able to know what kind of oscillatory behaviour is expected to ensure that the plant safety limits are not breached. In addition, the operator must get an appropriate and useful signal so as to take timely corrective action. These requirements can be met by the nonlinear stability (time domain) analysis. Nonlinear analysis is also required to establish a stable start-up, power raising and setback procedures in NCSs. Further, it may be noted that the analysis methodologies are the same for different systems like the steam generators, pressure tube type heavy water reactors, BWRs, etc. Therefore, first the analysis methodologies will be presented followed by a parametric analysis with a pressure tube type reactor as an example. Finally the considerations for start-up and the stability design of a NC BWR are dealt with briefly.

2. STABILITY ANALYSIS

Natural circulation systems can experience a large variety of instabilities as explained in the last chapter. Strictly speaking, NCS design must ensure stability for all types of instabilities. However, well-established analysis procedures do not exist for all observed instabilities. Fortunately, all types of instabilities are not observed in every natural circulation system. Hence, design procedures usually address only the commonly observed static and dynamic instabilities. Ledinegg instability and density wave oscillations (DWO) are the commonly observed static and dynamic instabilities respectively. Most NC based systems, require some continuous feed and bleed like the feed water flow and steam flow in a BWR. Since the location of feed and bleed points in the system has an important bearing on

the stability, it can be a design issue in some NCSs. In BWRs, neutronics plays a very important role in the thermalhydraulic instability. Hence BWRs require not only static and dynamic analysis but also coupled neutronic-thermalhydraulic analysis to arrive at the thresholds of instability. In short, we require analysis methods for
a) Static instability,
b) Dynamic instability and
c) Coupled neutronic thermal hydraulic instability.

3. STATIC INSTABILITY

3.1. Single-phase NCS

Most single-phase loops do not show pure static instability. The compound static instabilities associated with flow reversal in single-channel loops are analyzed in the same way as dynamic instabilities. Parallel channel systems also exhibit a static instability associated with flow reversal. Chato (1963) has developed a theoretical approach to calculate the critical power below which flow reversal is possible in a system of vertical unequally heated parallel channels. Similar approach can be used to develop a criterion for parallel horizontal channels or parallel vertical U-tubes. With horizontal heated channels as in PHWRs or vertical cooled U-tubes as in SGs, unequal driving forces exist even if all the channels are equally powered due to the difference in elevation and hence flow reversal possibility exists.

3.2. Two-phase systems

Compound static instability associated with flow reversal in two-phase single channel systems can be analyzed by dynamic stability analysis.

3.2.1. Ledinegg type instability

The instability is observed in the negative slopping region of the pressure drop vs. flow curve and the criterion for this type of instability is given by

$$\frac{\partial \Delta p_f}{\partial W} - \frac{\partial \Delta p_d}{\partial W} \leq 0 \tag{1}$$

Where Δp_f is the total pressure losses in the system and Δp_d is the driving head due to buoyancy. Δp_f includes all losses in the inlet piping, heat source, outlet let piping and steam drum except the pressure drop due to gravity in the downcomer, ($\Delta p_d = \rho g H$) (Fig. 1). To check the occurrence of Ledinegg instability, the variation of Δp_f and Δp_d as a function of flow rate is required. Since the down comer is in the single-phase condition, Δp_d does not vary with flow rate for a fixed inlet subcooling. Hence an equivalent criterion to the above is sometimes used:

$$\frac{\partial \Delta p_f}{\partial W} \leq 0 \tag{2}$$

The pressure loss for the loop in Fig. 1 can be written as

$$\Delta p_f = \frac{W^2}{A^2} \oint \partial v + g \int_{hi}^{SD} \rho dz + \frac{W^2}{2A^2 \rho_f} \left[K_i + \frac{f_f}{D} \left\{ L_{sp} + \left(\bar{\phi}_{Lo}^2 L_B \right)_h + \left(\phi_{Lo}^2 L_{tp} \right)_p \right\} + K_o \phi_{Lo}^2 \right] \tag{3}$$

Where the subscript hi refers to the heater inlet. Fig. 2 illustrates the use of the above criterion to identify the lower threshold for Ledinegg type instability. The calculations were actually performed for a configuration of the AHWR, which is a pressure tube type NC based BWR being designed in India (see Appendix-1). It shows that below a channel power of 0.285 MW, the system pressure loss characteristic intersects the driving buoyancy pressure differential only once indicating that only one operating point is possible. Above this power, the channel pressure loss characteristic intersects at three points indicating the existence of three operating points. In a similar way, the upper threshold can be identified. The lower and upper thresholds can be obtained similarly for other values of subcooling to generate the stability map as shown in Fig. 3. The instability is not observed below a certain subcooling for a given pressure. With increase in subcooling the unstable zone is found to increase and hence increasing the inlet subcooling has a destabilizing effect. It is found that as the pressure increases the unstable zone contracts as well as shifts up so that the easiest way to avoid this instability is to begin boiling at relatively higher pressures. In fact, it is found to shift beyond the operating envelope of power beyond a certain pressure.

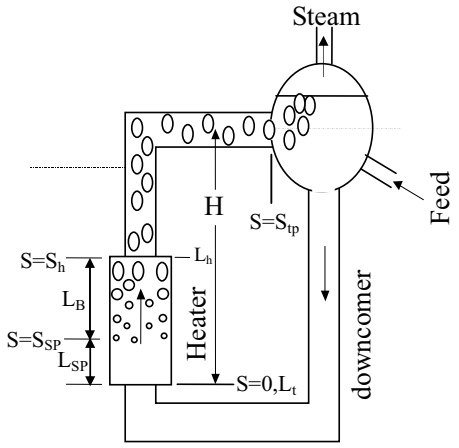

FIG. 1. Static instability in a two-phase NCS

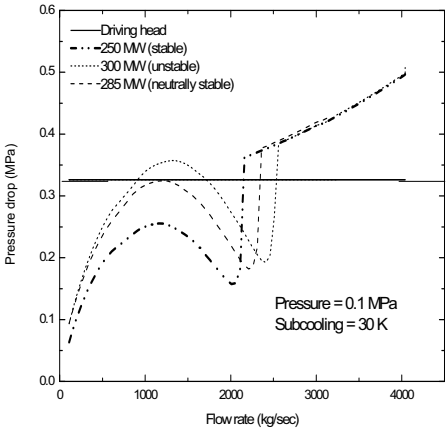

FIG.2. Identification of threshold values for Ledinegg type instability

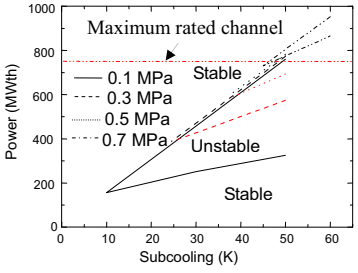

FIG..3. Effect of pressure on Ledinegg type instability

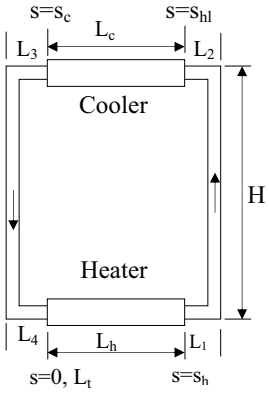

FIG..4. Geometry and coordinate system for a rectangular single-phase NCL

The predictions reported here on two-phase instability are carried out with the Baroczy (1966) model for two-phase friction multiplier. With increase of riser height, the unstable zone is found to enhance. Differences in power profiles do not make a major impact on the Ledinegg type instability in AHWR. A detailed parametric study of the instability can be found in Nayak et al (2000a).

3.2.2. Static Instability of Parallel Channel Systems

Parallel channel systems under two-phase flow condition, exhibit both kinds of multiple steady states: i.e. multiple steady states in the same flow direction as well as opposite flow directions. Linzer and Walter (2003) have theoretically studied flow reversal in a two-phase natural circulation system with unequally heated parallel vertical channels and proposed a criterion for flow reversal. Flow reversal under two-phase NC can be expected in horizontal parallel channels of the type used in pressure tube type PHWRs and vertical parallel U-tubes in steam generators. A criterion for flow reversal can be derived based on the theoretical approach proposed by Linzer and Walter (2003).

Several studies exist for the multiple steady states in the same flow direction (Ledinegg type instability). Rohatgi and Duffey (1998) obtained a closed-form solution for the stability of uniformly heated parallel channels based on the homogeneous equilibrium model. Considering the total pressure drop across a single channel as the sum of single-phase and two-phase region pressure drops, they obtained the following expression for the total pressure drop across a single channel

$$\Delta p = \frac{fW^2}{2DA^2}\left\{\frac{L_{sp}}{\rho_f} + \frac{L_h - L_{sp}}{\overline{\rho}_m}\right\} + \frac{W^2}{2A^2}\left\{\frac{K_i}{\rho_f} + \frac{K_o}{\rho_m}\right\} + g\left\{L_{sp}\rho_f + \left(L_h - L_{sp}\right)\overline{\rho}_m\right\} \tag{4}$$

Differentiating the above and using the condition of static instability as $\frac{\partial \Delta p}{\partial W} = 0$, they obtained the following nondimensional equation for the static instability of parallel channels.

$$N_p^2 N_{fr}\left(1 + \overline{K}_o\right) + 2N_p N_{fr}\left[\left(1 - N_s\right)\left(2 + \overline{K}_o\right) + \overline{K}_i\right] + 3N_{fr}N_s^2 + 2N_f\left(2 + N_s\right) = 0 \tag{5}$$

The instability region is bounded by the two roots of the above equation and hence provides a method for obtaining the region of instability. The stability map obtained from Eq. (5) is similar to that given in Fig. 3.

4. DYNAMIC INSTABILITY

Dynamic instability of the density wave type is the most commonly observed instability for both single-phase and two-phase natural circulation loops. In general, the dynamic stability analysis is performed either by the linear or the non-linear method.

4.1. Linear Stability Method

In the linear stability method, the time dependent governing equations are perturbed over the steady state. The perturbed equations are linearized and solved analytically to obtain the characteristic equation for the stability. The roots of the complex characteristic equation are then obtained numerically and the stability is judged by the Nyquist stability criterion. As per this criterion, if any of the roots of the characteristic equation has a positive real part, then the corresponding operating conditions are unstable. The marginal stability curves, which separate the stable and unstable zones, can be obtained in this way for both single-phase and two-phase loops. This method is also known as frequency domain analysis and is best suited for generating the stability map. The method is computationally less expensive and gives exact analytical solution of the linearized governing equations and is free from numerical stability problems. The mathematical derivation of the characteristic equation, however, is a tedious process.

4.1.1. Linear Analysis of Single-phase NCSs

For a specified uniform diameter rectangular loop, the maximum steady state flow rate for a given power and cooler secondary conditions is achievable with horizontal heater and horizontal cooler (since it has the largest elevation difference) compared to any other orientation of heat source and heat sink. However, it does not tell us whether that particular steady state is stable. Experiments indicate that this is the least stable orientation of heater and cooler. Thus stability analysis is necessary to examine whether a particular steady state is stable or not. To illustrate the linear analysis technique, we consider the simple uniform diameter rectangular loop shown in Fig. 4. The integral momentum equation applicable to one-dimensional single-phase flow in nondimensional form is (see Appendix-2 for the derivation).

$$\frac{d\omega}{d\tau} = \frac{Gr_m}{\mathrm{Re}_{ss}^3} \oint \theta \, dZ - \frac{pL_t \omega^{2-b}}{2D\,\mathrm{Re}_{ss}^b} \tag{6}$$

Similarly, the nondimensional energy equation applicable for the various segments of the loop can be written as

$$\frac{\partial\theta}{\partial\tau} + \phi\omega\frac{\partial\theta}{\partial S} = \begin{Bmatrix} \dfrac{L_t}{L_h} & heater & \left(for\ 0 < S \le S_h\right) \\ 0 & pipes & \left(for\ S_h < S \le S_{hl}\ and\ S_c < S \le S_t\right) \\ -St_m\theta & cooler & \left(for\ S_{hl} < S \le S_c\right) \end{Bmatrix} \tag{7}$$

During linear stability analysis, we slightly perturb the flow rate and temperature over the steady state as follows:

$$\omega = \omega_{ss} + \omega' \ and\ \theta = \theta_{ss} + \theta' \quad where \quad \omega' = \bar{\omega}\varepsilon e^{n\tau} \ and\ \theta' = \bar{\theta}(S)\varepsilon e^{n\tau} \tag{8}$$

From the above, it is clear that knowledge of the exact steady state flow rate and temperatures are essential for performing the linear stability analysis. The steady state solutions of equations 6 and 7 for rectangular loops can be found in Appendix-2. The same can be extended to any single-phase loop as shown by Vijayan et al. (2004a). Substituting Eq. (8) into Eq. (6) and (7), the perturbed equations are obtained. Linearizing and solving the perturbed equations analytically, the characteristic equation for the stability parameter, n is given by (see appendix-3 for the derivation)

$$n - \frac{(p/2)^{1+m}}{(Gr_m I_{ss})^m (D/L_t)^{1+m}} \left[\left(\frac{\bar{I}/\bar{\omega}}{I_{ss}} \right) - (2-b) \right] = 0 \tag{9}$$

$$Where \quad \frac{\bar{I}}{\bar{\omega}} = \frac{1}{\bar{\omega}} \oint \bar{\theta}(S)\, dZ \tag{10}$$

For the rectangular loop with horizontal heater and cooler, we obtain the following expression after integration (see Appendix-3)

$$\frac{\bar{I}}{\bar{\omega}} = \frac{\phi}{n}\left(1 - e^{\frac{-n}{\phi}}\right)\left\{ \frac{\bar{\theta}_h}{\bar{\omega}} e^{\frac{-nL_1}{L_t}} - \frac{\bar{\theta}_c}{\bar{\omega}} e^{\frac{-nL_3}{L_t}} \right\} \tag{11}$$

If $L_1=L_3=L_x$, then, $$\frac{\bar{I}}{\omega} = \frac{\phi}{n}\left(1-e^{\frac{-n}{\phi}}\right)e^{\frac{-nL_x}{L_t}}\left\{\frac{\bar{\theta}_h-\bar{\theta}_c}{\bar{\omega}}\right\} \quad (12)$$

Which is same as that in Vijayan (2002). The expression for $(\bar{\theta}_h-\bar{\theta}_c)/\bar{\omega}$ can be found in Appendix-3. The characteristic equation is a complex transcendental equation in terms of the stability parameter n. To assess stability, either we search for the roots of this equation using a numerical technique or make Nyquist plots (Fig. 5a). The former method is more popular.

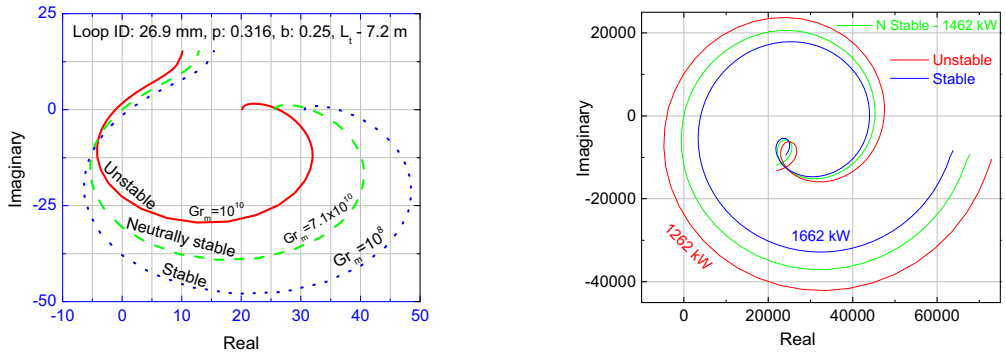

(a) Single-phase loop (b) Two-phase loop

FIG..5: Nyquist plots for single-phase and two-phase loops

TABLE-1: COMMONLY USED LINEAR STABILITY ANALYSIS CODES

Name of code	Thermalhydraulic model		Neutronics model	Reference
	Channels	TPFM (Eq)		
NUFREQ NP	A few	DFM (4)	P-K[1], 1-D, 2-D & 3-D	Peng (1985)
LAPUR6	1-7	HEM (3) & Slip Model	P-K[1], M-P-K[2] & 1-D	Muñoz-Cobo (2006)
STAIF	10	DFM (5)	1-D	March-Leuba (2000)
FABLE	24	HEM (3)	P-K[1] with void reactivity from PANACEA 3-D data	Hănggi (2001)
ODYSY	A few	DFM (5)	1-D with PANACEA 3-D data	D'Auria (1997)
MATSTAB	All	DFM (4)	3-D	Hănggi (2001)

[1] P-K: point kinetics; [2] M-P-K: modal point kinetics; TPFM: two-phase flow model

4.1.2. Linear Analysis of Two-phase NCSs

The principles of linear stability analysis are same for single- and two- phase natural circulation systems. The stability criterion (Nyquist criterion) and the procedure for searching the roots of the complex characteristic equation and making Nyquist plots (Fig. 5b) are also the same. However, the governing equations are somewhat different for the two-phase regions of the system depending on the chosen equation system. For two-phase flow, one can make a wide choice starting from the homogeneous equilibrium model, which uses one equation each for the mass, momentum and energy conservation similar to single-phase flow. However, it is well known that there is a difference in the velocity between the vapor and liquid phases. The simplest model that takes care of this difference in velocity is the drift flux

model (DFM). In many two-phase flow situations, the temperature of the liquid and vapor phases can be different as in subcooled boiling and droplet flow. Considering both thermal and kinematic nonequilibrium require application of the conservation laws to each phase (two-fluid model). Most two-fluid models are mathematically ill posed rendering them unsuitable for instability analysis. As a result linear stability analysis with the two-fluid model was not available till recently. Zhou and Podowski (2001) have carried out a frequency domain analysis of the two-fluid equations for the first time. Recently Song and Ishii (2001) proposed a well-posed two-fluid model (TFM) with certain restrictions on the liquid and gas momentum flux parameters. Thus, one can use the simple homogeneous model to a two-fluid model for analyzing two-phase flow instability. Table-1 demonstrates the equation system used in the various codes for stability analysis. Consideration of all these models is beyond the scope of this course. The linear analysis of two-phase flow instabilities is illustrated with the homogeneous equilibrium model (HEM) in Appendix-4.

4.1.3. Parallel Channel Instability

The linear stability analysis described in Appendix-4 also includes the effect of parallel channels. For parallel channel instability, it is also of interest to know whether the oscillations are in-phase or out-of-phase. From the solution of the characteristic equation, we can estimate the ratio

$$\frac{\left(W_{in}^{'}\right)_i}{\left(W_{in}^{'}\right)_j} = \frac{G_j}{G_i} = M + jN \tag{13}$$

Where G_i is the sum of perturbed pressure drops in the i^{th} channel. The quantity M+jN can be expressed as $Re^{j\theta}$ where the ratio of the amplitudes, R, is obtained as $R = \sqrt{M^2 + N^2}$ and the phase difference, θ, is obtained as $\theta = \tan^{-1}\left(N/M\right)$. Depending on the value of θ the oscillatory nature can be identified as in-phase or out-of-phase.

4.1.4. Coupled Neutronic Thermalhydraulic Instability

In nuclear reactors, as the void fraction fluctuates, it also affects the neutronics via the void reactivity feedback resulting in power oscillations. It may be noted that if the void reactivity coefficient is zero, then the neutron kinetics and thermalhydraulics are decoupled and the instability threshold can be predicted from a pure thermalhydraulic model as in the case of a thermalhydraulic test facility. But in most BWRs, the void reactivity is significantly negative and a coupled stability analysis considering both neutronics and the thermal hydraulics are essential.

As we have seen in the last lecture, several modes of power oscillations such as global (in-phase), regional (out-of-phase) and local are possible in a nuclear reactor. It is easy to note that the analysis requirements are also different for the different oscillatory modes. For example, the in-phase mode can be easily analyzed with a point kinetics model. However, the point kinetics model can only give approximate results in case of axial power variation and 1-D kinetics model is better. The analysis of out-of-phase oscillations, in principle, requires a 3-D kinetics model. The major problem in linear analysis of the 3-D kinetics equations is very complex mathematics with a lot of approximations. Hence, several simplified treatments relying on multi-point kinetics and modal kinetics are available for the analysis of out-of-phase instability. Linear stability analysis considering 3-D kinetics model is beyond the scope of the present course. Both multi-point kinetics and modal kinetics are briefly described in Nayak et al. (2000a and b).

4.2. Nonlinear Stability Analysis

Linear analysis tells us whether a particular steady state is stable or unstable and is well suited to generate a stability map. It does not tell us how the steady state can be approached. Stability thresholds of a NCS, depends on the way we approach the steady state due to the hysteresis effects (Chen et al. (2001)) or conditional stability (Vijayan et al (2004b)). In other words, stability threshold depends on the operating procedure. Achard et al. (1985) also show that finite amplitude perturbation can cause instability on the stable side of the linear stability boundary. Hence, nonlinear analysis is required to establish the stable operational domain and start-up procedure for NC based BWRs. This is carried out by the time domain codes which numerically solve the governing nonlinear partial differential equations directly. Usually such codes are based on the finite difference method where the results depend on the space and time steps employed and are not free from numerical instability problems. The stability analysis is carried out just like a normal transient analysis with the steady state conditions as the initial conditions. It is usual practice to perturb (but is not essential) one of the dependent variables like flow and track the behaviour of the disturbance. If the disturbance dies down with time, it is stable and if it oscillates with the same amplitude, it is neutrally stable and if it grows with time, then it is unstable. Nonlinear stability analysis is required to obtain the nature of the oscillatory behaviour like magnitude of the temperature and flow oscillations. They are capable of predicting the limit cycle oscillations and higher harmonic modes of oscillation. Generally both frequency domain and time domain codes are required for the complete stability analysis and establishing the operating and start-up procedure of NC BWRs.

Nonlinear analysis can, in principle, be carried out by codes used for the normal transient thermalhydraulic analysis of nuclear reactors (Table-2). For example, Vijayan et al. (1995) used the ATHLET code to simulate the single-phase natural circulation instability in a rectangular loop. Ambrosini and Ferreri (1998), Misale et al. (1999) and Manish et al. (2002) and (2004)) used the RELAP5 code for single-phase instability analysis of rectangular loops. Misale et al. (1999) have also used the CATHARE code for the same. There are also time domain codes dedicated to stability analysis like RAMONA-5.

TABLE-2: COMMONLY USED CODES FOR NONLINEAR STABILITY ANALYSIS

Name of code	Thermal hydraulic model		Neutronics model	Reference
	Channels	TPFM (Eq.)		
RAMONA-5	All	DFM (4 or 7)	3-D	RAMONA-5 catalogue
RELAP5/MOD 3.3	A few	TFM (6)	P-K & 3-D PARCS	Relap5 (1995)
RELAP3D	Multiple	TFM (6)	3-D (NESTLE)	INEEL-EXT-98-00834 Rev. 2.4
RETRAN-3D Mod 4.3	4	Slip (5)	P-K, 1-D & 3-D	www.csai.com
TRACG	A few	TFM (6)	3-D	Takeuchi (1994)
ATHLET	A few	TFM (6)	P-K, 1-D, 3-D (QUABOX-CUBBOX/DYN3D)	Lerchl (2000)
CATHARE	A few	TFM (6)	P-K	Barre (1993)
CATHENA Mod-3.5d	A few	TFM (6)	P-K	Beuthe & Hanna (2005)

4.2.1. Single-phase NCSs

While using large system codes for single-phase instability analysis, the reported experiences appear to vary significantly. With the ATHLET code Vijayan et al. (1995) found that the adopted nodalization plays a very important role. Coarse nodalization led to stable steady flow always. With relatively finer nodalization, instability was observed and reasonable simulation of the essential features of the single-phase instability was possible. While reproducing the results of Welander (1967) using RELAP5, Ferreri and Ambrosini (2002) found that depending on the node size used the

code can predict stability or instability. Manish et al. (2002 & 2004) also reported similar dependency on nodalization while using RELAP5/MOD3.2 code. Manish et al. were able to reasonably reproduce the steady state flow rate and the instability threshold for a particular nodalization. However, if the nodalization is made finer then it is found that no steady state solutions exist. Ambrosini and Ferreri (1998) studied the effect of various numerical schemes with different order of accuracy and found that second order schemes were better in reducing truncation error. Misale et al. (1999) reported that the CATHARE code was able to predict the steady state quantities, but failed to show instability. On the other hand RELAP code is able to show instability but not at the same power levels as in the experiments. The main drawback of these codes is that they are somewhat unwieldy for the analysis of instability of single-phase natural circulation in simple loops. However, simpler codes for the same purpose can be easily developed, a theoretical formulation for which is given in Appendix-5. The nodalization related problem is found to exist even with such simple codes (Vijayan et al. (2004b)) and the predicted instability threshold was found to be much lower than the experimental values. However, the steady state flow rates could be predicted with reasonable accuracy. Even though the time series of the observed unstable flow regimes could be predicted, the shape of the limit cycles was significantly different. The deviations were attributed to the 3-D effects and the use of fully developed friction factor correlations for the unstable oscillatory flow where the flow is never fully developed.

4.2.2. Two-phase NCSs

Several formulations for the nonlinear stability analysis based on the homogeneous model are reported in the literature. Typical examples are those given by Chatoorgoon (1986) and Chang and Lahey (1997). Again, codes used for the normal transient thermalhydraulic analysis are applicable for nonlinear stability analysis of two-phase NCSs. Most codes, however, use a point kinetics model which is sufficient for the analysis of in-phase instability but not good enough for the analysis of out-of-phase instability. The problem is overcome in most commercial codes by coupled analysis with a 3-D neutronics code. There are also time domain codes like RAMONA-5 with 3-D neutronics, which may be used for the analysis of out-of-phase instability.

5. PARAMETRIC EFFECTS ON THE DWI IN SINGLE-PHASE NCS

DWI is the most commonly observed instability in NCLs. Although there are a large number of identified mechanisms for instability, almost all of them ultimately lead to the occurrence of DWI in a single-phase loop. It may be noted that a generalized nondimensional correlation valid for steady state flow in uniform and nonuniform diameter single-phase natural circulation loops has been presented in Vijayan et al. (2004a). However, even for uniform diameter single-phase loops, there does not exist a universal stability map. Instead it depends on a large number of parameters as listed below.

$$Stability = f(Gr_m, St_m, \frac{L_t}{D}, orientation, length\ scales, flow\ regime\ and\ direction) \qquad (14)$$

The orientation includes, horizontal heater and horizontal cooler (HHHC), horizontal heater vertical cooler (HHVC), vertical heater horizontal cooler (VHHC) and vertical heater and vertical cooler (VHVC). The length scales include, L_t/H, L_t/L_h, L_c/L_t, L_{hl}/L_t, L_{cl}/L_t, L_1/L_t, L_2/L_t, L_3/L_t and L_4/L_t. The flow regime includes both laminar and turbulent and flow direction includes both clockwise and anticlockwise. A detailed study of all these parameter is available in Vijayan et al. (2001).

5.1. Effect of orientation of source and sink

It may be noted that different reactor concepts use different orientations of the heat source (i.e. core) and sink (i.e. steam generator). The effect of the orientation of the source and sink is studied in a simple uniform diameter rectangular loop (Fig.6). With clockwise flow, the VHVC orientation is most stable and HHHC orientation is least stable (Fig. 7). For a given heater orientation, the horizontal cooler orientation is less stable compared to the vertical

cooler. Similarly, with fixed cooler orientation, the loop with vertical heater is more stable than that with horizontal heater. All these four orientations were experimented in a uniform diameter rectangular loop (Fig. 6) and instability could be observed only for the HHHC orientation.

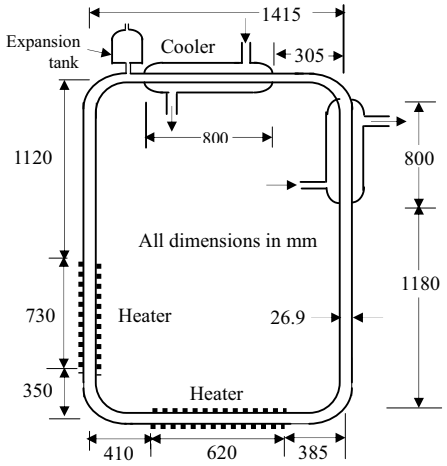

FIG. 6. Schematic of experimental loop

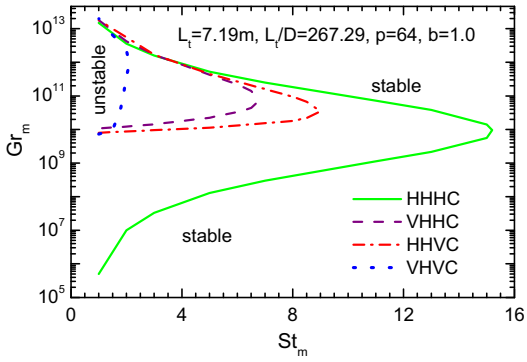

FIG. 7. Effect of heater and cooler orientation on the stability

5.2. Effect of Heater and Cooler Lengths

These studies were carried out for the HHHC orientation with clockwise flow for the loop in Fig. 6 by changing the heater or cooler lengths keeping the loop height and width the same. The results for varying the heater length alone and cooler length alone are given in figures 8a and b respectively. It is found that reducing the length of heater or cooler has a destabilizing effect. However, the heater length has only a marginal effect on the stability behaviour whereas the cooler length has a significant effect.

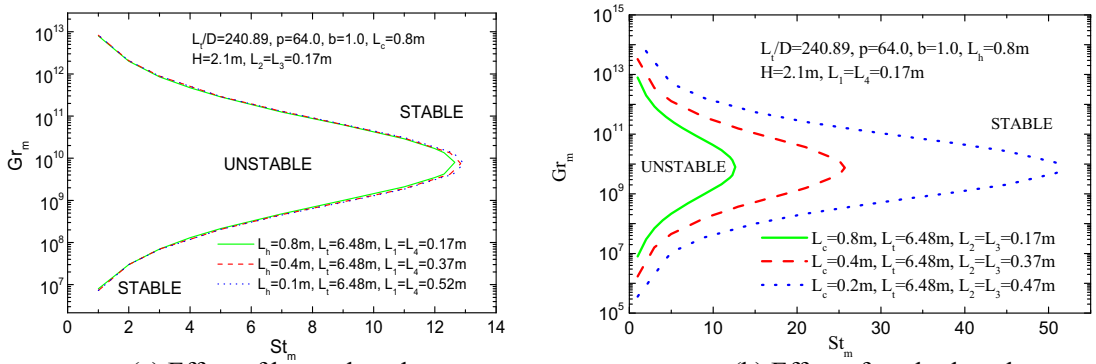

(a) Effect of heater length (b) Effect of cooler length

FIG. 8. Effect of heater and cooler length on stability

5.3. Effect of L_t/D

It may be noted that L_t/D is the contribution of the loop geometry to the friction number in a uniform diameter loop. Also, most techniques for stabilization results in enhanced L_t/D. A typical example is the introduction of orifices (Misale and Frogheri (1999)). Increasing L_t/D stabilizes the loop flow

(Vijayan and Austregesilo (1994)). Both the lower and upper thresholds are found to increase with L_t/D (Fig.9). It may be noted that single-phase NC instability has been observed in loops with low L_t/D (<500). Most reactor loops operate with L_t/D in the range of several thousands and that is the main reason why single-phase instability is not observed in reactors.

5.4. Effect of flow regime

With the flow regime changing from laminar to turbulent, the constants p and b in the equation for friction factor changes and it has a significant influence on the stability behaviour (Fig.10). Good agreement with experimental data can be obtained with empirical friction factor correlation (Vijayan et al. (1992) and Vijayan and Austregesilo (1994)).

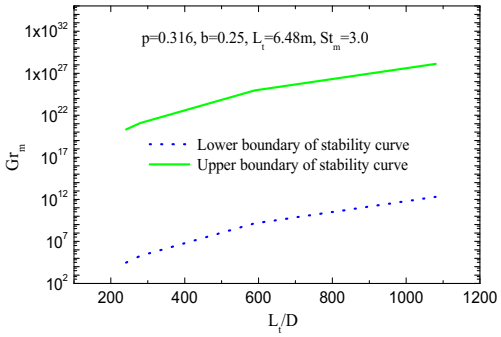

FIG. 9. Effect of L_t/D on the instability

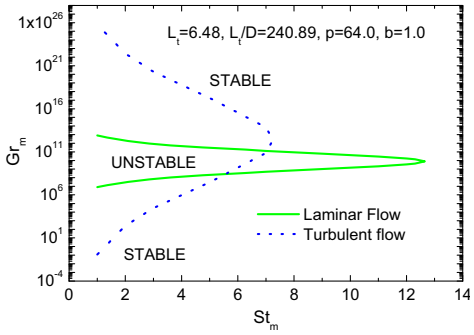

FIG.. 10. Effect of flow regime

5.5. Effect of flow direction

In case of HHVC orientation, it appears possible from the steady state analysis to have flow in the clockwise or anticlockwise direction. However, from the stability analysis, it may turn out that no stable operation is possible with flow in the anticlockwise direction for certain loops. The derivation of the characteristic equation for the stability behaviour can be found in Appendix-3.

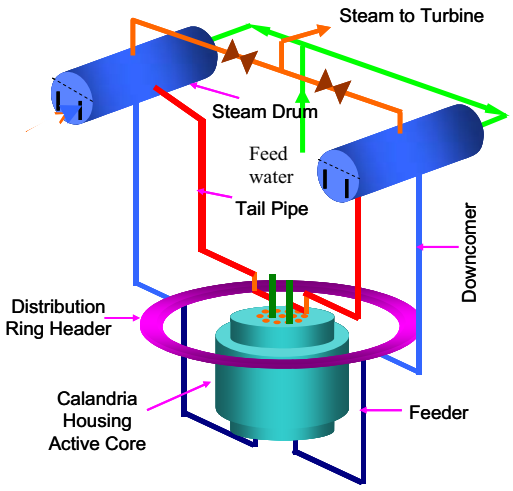

FIG.11: Schematic of AHWR main heat transport system

6. PARAMETRIC EFFECTS ON THE DWI IN TWO-PHASE NCSS

It may be noted that there does not exist a universal stability map valid for all loops. Under these conditions, it is only possible to examine the parametric effects to obtain general trends of the stability behaviour of NCSs. The parameters affecting two-phase flow instability can be classified into two:

operating parameters and design parameters. The operating parameters include the inlet subcooling, pressure, heater power and its distribution. Design parameters include the loop geometry, the working fluid and the flow rate. Knowledge of the parametric dependence is useful in understanding the instability and to develop techniques for avoiding it. The parametric dependences of forced circulation BWRs are well known. In the following, parametric dependence of a pressure tube type natural circulation boiling water reactor is illustrated with results from the AHWR (Fig.11).

6.1. Effect of Inlet Subcooling and Pressure

As the inlet subcooling increases, the lower instability threshold is found to increase where as the upper threshold is found to decrease. The net effect is that the gap between the two thresholds (i.e. the stable region) decreases. Thus inlet subcooling has a destabilizing effect. The effect of pressure on the NC density wave instability is significant (see Fig. 12). Increase in system pressure enhances the area of the stable zone considerably. Hence pressure has a stabilizing effect on the two-phase density wave instability.

6.2. Effect of Riser Height

It may be mentioned that the riser height has a significant influence on the steady state flow rate. Riser height is found to enhance the steady state flow rate. However, its effect on the stability is rather interesting (Fig. 13). It has a stabilizing influence up to a certain value of the riser height. Beyond that it has a destabilizing influence due to its contribution to the two-phase pressure drop.

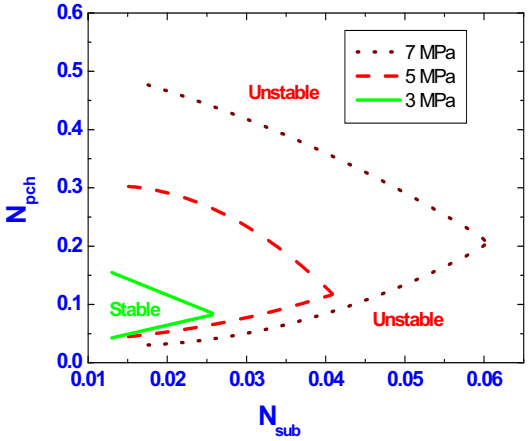

FIG. 12. Effect of pressure on DWI

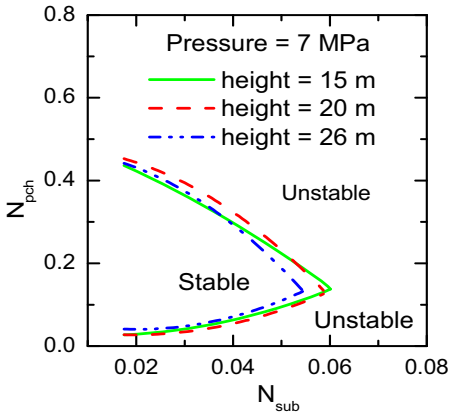

FIG.13. Effect of riser height on DWI

6.3. Effect of Downcomer Level

During a small break LOCA as the inventory loss continues the downcomer level decreases with time. Reducing the downcomer level has a significant destabilizing effect as it directly reduces the single-phase pressure drop (Fig.14).

6.4. Effect of Outlet Orificing

Enhancing the loss coefficients in the two-phase regions has a large destabilizing effect. Even for a pressure tube type reactor this is found to be true (see Fig. 15).

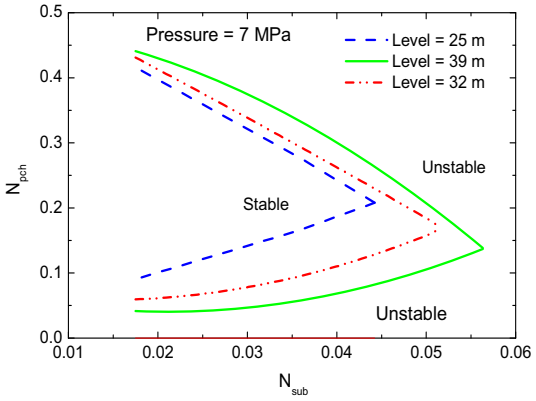

FIG.14. Effect of downcomer level on DWI

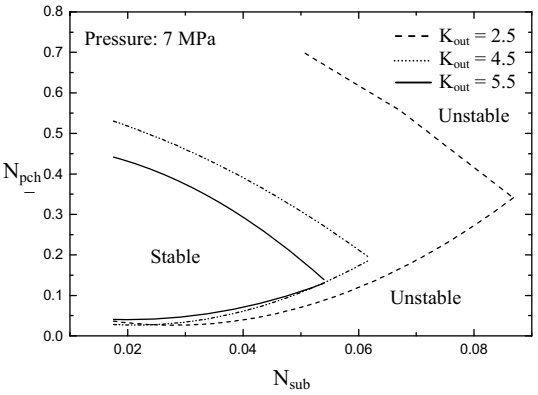

FIG.15. Effect of outlet orificing on DWI

6.5. Effect of Parallel Channels

With the inclusion of parallel channels in the analysis, both in-phase and out-of-phase oscillation (OPO) modes are possible. The OPO is the unique characteristic of parallel channel instability. However, the effect of number of channels on the threshold of OPO needs to be established first as out-of-phase mode oscillations are possible with any number of parallel channels. Analysis was carried out for 2, 5, 8 and all parallel channels for AHWR by Nayak et al. (1998, 2000a, 2000b & 2002). The results indicated that a conservative prediction of parallel channel instability could be made with the maximum rated twin channel system (Fig. 16). Hence all subsequent results presented here are for the twin channel system. It may also be noted that this result is of great significance even for experimental validation as all relevant stability data can be generated with a twin channel system.

6.6. Unstable Oscillatory Regimes with Parallel Channels

A comparison of the in-phase and out-of-phase instability thresholds is shown in Fig. 17 (the numbers on the curves show the oscillation frequency). With this plot, it is easy to identify the zone of OPO and dual oscillations as shown in the figure. In the dual oscillation regime, the natural circulation system is susceptible to both in-phase and out-of-phase oscillations. Van der Hagen et al. (1994) and Pazsit (1995) reported the occurrence of dual oscillations in BWRs. One characteristic feature of dual oscillations is that the decay ratio will show discontinuous behaviour, as both oscillation modes are dormant. It is found that the stable zone for the OPO is significantly lower than the stable zone of IPO. In other words, the out-of-phase instability is controlling. It may be recalled here that in forced circulation BWRs (e.g. Lasalle), out-of-phase instability was observed following the loss of all circulating pumps.

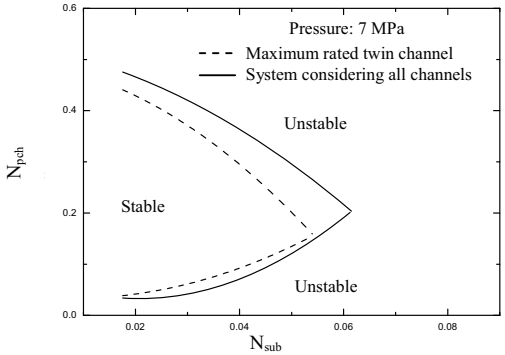

FIG.16. Effect of number of channels on OPO

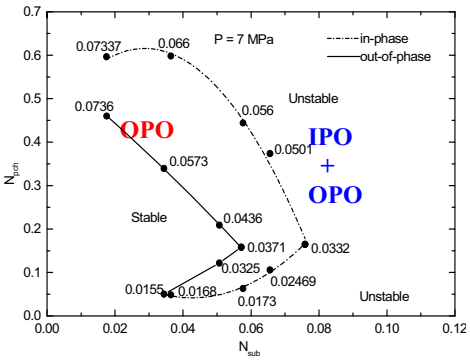

FIG. 17. Comparison of stability maps for IPO and OPO

6.7. Effect of Inlet Orificing

Inlet orificing is always found to stabilize forced circulation BWRs. Even in AHWR, if all channels are uniformly orificed, then it is found to increase stability (Fig. 18a). However, in case of parallel channel systems, uniform orificing is rarely possible. In fact the high power channels are not orificed at all. The effect of increasing the inlet loss coefficient of one channel of a twin channel system is shown in Fig. 18b. It is found that increasing the inlet loss coefficient beyond a certain value is destabilizing. This is again characteristic of natural circulation systems, as the driving force is limited.

6.8. Coupled Neutronic Thermalhydraulic Instability

So far we have not considered the effect of neutronics on the stability behaviour. Its effect, however, is important in the design of both forced and natural circulation based BWRs.

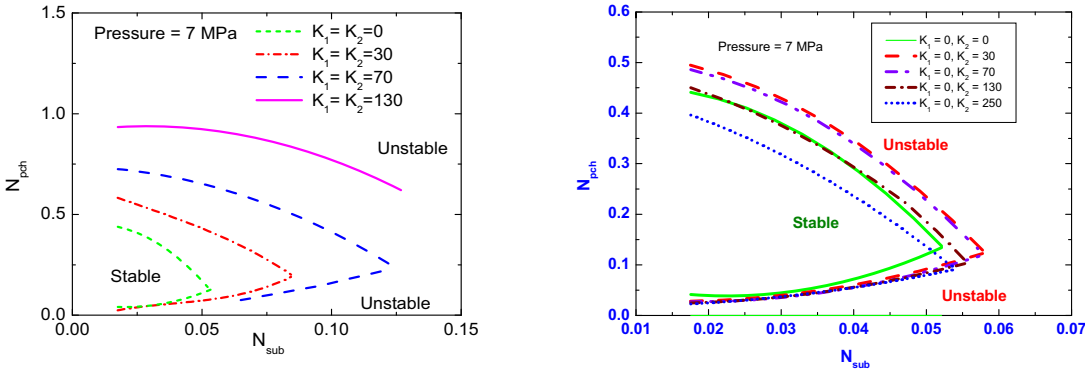

(a) Uniform orificing *(b) Nonuniform orificing*

FIG. 18. Effect of inlet orificing on OPO

6.8.1. Effect of Void Coefficient

It may be noted that if the void coefficient is zero, then there is no coupling between neutronics and thermal hydraulics and hence the stability map so obtained is identical to the pure thermalhydraulic stability map. Negative void coefficient stabilizes both in-phase and out-of-phase oscillations so that pure thermalhydraulic stability map is found to be conservative for AHWR (Fig. 19). It may be mentioned that the value of void coefficient is significantly higher at low pressures and hence with neutronics, the influence of pressure on instability is amplified. Since the effect of neutronics on in-phase and out-of-phase instability show the same trend, henceforth we focus our attention to the out-of-phase instability only.

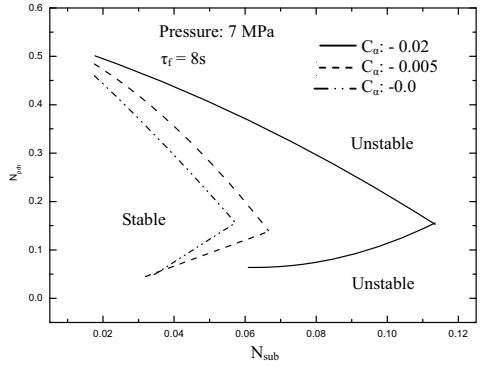

FIG. 19. Effect of void coefficient on OPO

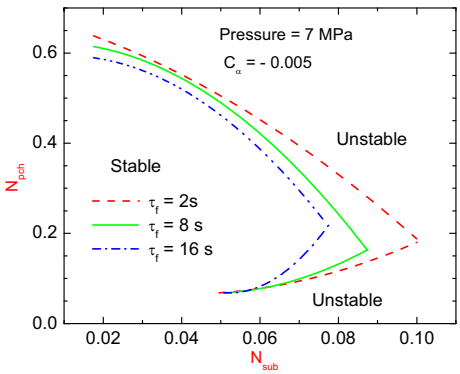

FIG. 20.Effect of fuel time constant on OPO

6.8.2. Effect of Fuel Time Constant

Apart from fuel properties, the burn up also affects the fuel thermal time constant. Larger time constants have a destabilizing effect on the out-of-phase instability (Fig. 20). The same trend is observed in forced circulation BWRs.

6.8.3. Effect of Coupling Coefficient

The above results have been obtained using a point kinetics model. As already explained, the point kinetics model is good enough only for the in-phase instability. During an out-of-phase instability interaction among the parallel channels may affect the stability thresholds. The simplest way to consider its effect is to assume that the core consists of two subcores. The degree of coupling between the subcores is defined in terms of the coupling coefficient. For use in coupled multi-point kinetics, the coupling coefficients are to be evaluated separately using more sophisticated codes. Results indicate that a large value of the coupling coefficient reduces stability (Fig. 21).

6.8.4. Comparison of Coupled Multi-point and Modal Point Kinetics Models

The modal point kinetics model can also predict the out-of-phase instability. Based on the methodology of Turso et al. (1997), the subcriticality can be calculated. Corresponding to this subcriticality, the coupling coefficient can be calculated from the theory of Nishina and Tokashiki (1996). A comparison of the stability maps so predicted by the multipoint and modal point kinetics models is given in Fig. 22.

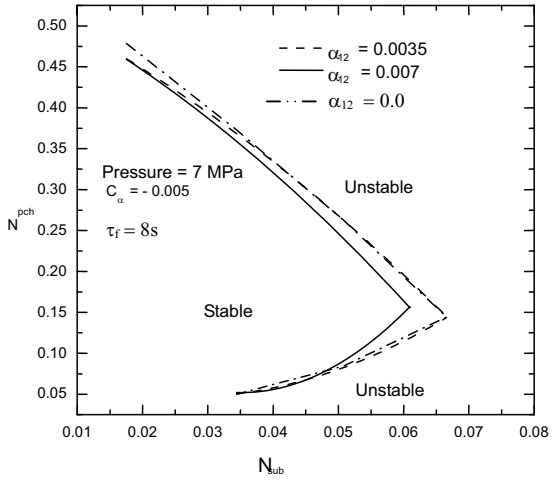

FIG. 21. Effect of coupling coefficient on OPO

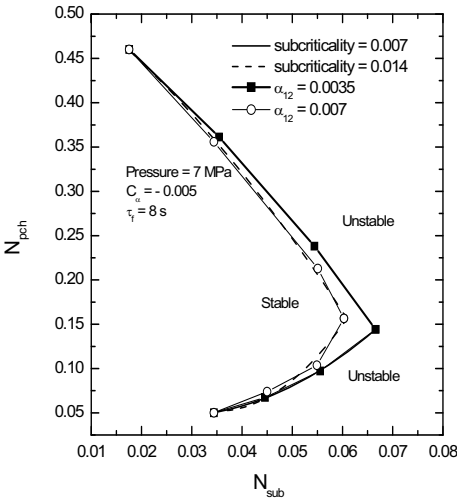

FIG. 22. Comparison of multi-point and modal point kinetics models

7. NONLINEAR ANALYSIS

As already pointed out nonlinear or time domain analysis is required for obtaining the nature of the oscillatory behaviour such as the mode, periodicity, direction and amplitude of oscillations. It can also predict the time series and limit cycle of oscillations.

7.1. Single-phase Natural Circulation

Nonlinear analysis can be carried out with any initial condition. Using the steady state initial condition, the predicted stability map using the nonlinear method was essentially the same as that obtained using the linear stability method.

7.1.1. Oscillatory Modes

Nonlinear analysis can also be used to investigate the oscillation modes and the limit cycles. Experimentally only three oscillatory modes were observed for rectangular loops. They are periodic unidirectional pulsing, chaotic switching between unidirectional and bi-directional pulsing and periodic bi-directional pulsing. Using the nonlinear code, it was possible to obtain the three different oscillatory modes, albeit at somewhat different conditions (Manish et al. (2002)). Detailed study of the temperature profile showed that both unidirectional and bi-directional oscillations have 3 dense and light pockets each at any instant differing only in magnitudes resulting in the different oscillatory modes (Vijayan et al. (2007)).

In low pressure experimental loops, it is not possible to obtain the full spectrum of the oscillatory modes in the single-phase condition as it leads to boiling with increase in power. With the nonlinear code, however, it is possible to do so and it was found that even the simple rectangular loop exhibits a rich variety of oscillatory modes (Manish et al. (2002)).

7.2. Two-phase Flow

Nonlinear codes are extensively used to study the characteristics of in-phase and out-of-phase instability in BWRs (Maqua et al.). It has also been used to analyze the chaotic behaviour in two-phase natural circulation loops (Chang and Lahey (1997)), parallel channel behaviour (Aritomi et al. (1986)). Dimmick et al. (2002) used the nonlinear code to obtain the stability boundaries of a supercritical reactor. For NC BWRs, due to the possibility of the hysteresis phenomenon, nonlinear analysis codes are used to establish stable operating procedures and start-up procedure. Nonlinear codes are used to study the effect of various initial conditions and operating procedures on the instability. Their use in establishing the start-up procedure of NC based reactors is discussed in the following section.

8. NC BASED PRESSURE TUBE TYPE REACTORS

Although, there are several NC based BWRs being developed in many countries, most of them are vessel type BWRs. The Advanced Heavy Water Reactor (AHWR) is the only one using the pressure tube concept. Other pressure tube type BWRs like the Fugen operate in the natural circulation mode only when the pumps fail. From the results of the parametric studies reported earlier, the stability behaviour in a pressure tube type BWR is found to be similar to that of vessel type BWRs. The issues during start-up and power raising are also expected to be similar. However, unlike vessel type BWRs the pressure losses in the inlet and outlet piping can have an influence on the steady state and stability behaviour. Hence size optimization of the inlet and outlet piping is an important design aspect of pressure-tube type reactor. In pressure tube type NC BWRs, the riser height is relatively large leading to much lower frequency of density wave oscillations. The stability issue significantly influences the start-up procedure for NC based BWRs. Detailed investigations were carried out for both the start-up and the power raising procedures for AHWR.

8.1. Design Procedure

One of the considerations in a pressure tube type reactor at the design stage is the sizing of the inlet and outlet pipes. Larger pipe sizes decrease the frictional resistance and hence increase the flow rate. On the other hand large pipe sizes increases the capital cost. Often, pipe size has opposing influences on the CHF and stability of the system. For example, reducing the inlet pipe size can enhance stability but reduces the flow rate and hence increases the exit quality leading to a reduction in the CHF. An optimization of pipe sizes is therefore required for natural circulation systems.

8.2. The Issues during Start-up and Power Raising

The basic issues during the start-up of a natural circulation based BWR is the avoidance of flow reversal and overcoming the lower threshold of the density wave instability. Experience with natural circulation boilers suggests that flow reversal is a problem in case of hot start-up (Linzer and Walter (2003)). The problem with the down flowing heated channels is that they supply steam to the inlet header and the downcomer, which has a destabilizing effect on natural circulation. The studies by Chato (1963) and Linzer and Walter shows that flow reversal is expected to occur only at very low powers. Above a critical power ratio the flow reversal phenomenon is not expected. This critical power ratio can be readily calculated using the maximum and minimum rated channels. The problems associated with flow reversal can be avoided by ensuring that boiling is initiated only above this power.

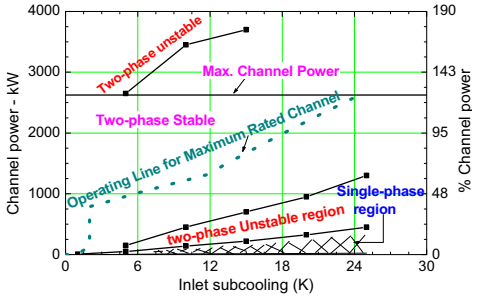

FIG. 23. Stability map for OPO in AHWR

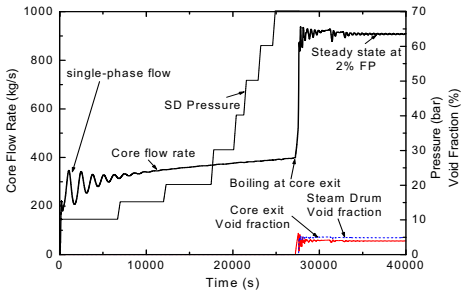

FIG.24. Start-up with stage-wise pressurization

The lower threshold of stability occurs at relatively high power at the inlet subcooling corresponding to the full power condition. It happens at around 60 to 70 % FP in the currently operating BWRs if the flow comes down to about 40%. In AHWR, if the subcooling remains same as at full power condition, then the corresponding stability threshold is approximately 50% FP (Fig. 23). As the reactor is to be started up from cold condition (very high subcooling), the lower threshold has to be overcome without initiating instability. Fig. 20 shows that the lower threshold decreases with reduction in subcooling and below about 5^0C the lower threshold occurs at very low power. Also, the lower threshold of instability does not exist for very low subcooling at the full pressure. Hence, there are several options for the start-up. Two options being pursued for AHWR are

a) Stage-wise pressurization using an external boiler and heat up with low reactor power. In this scheme, boiling is initiated at the full pressure and a very low subcooling at which the instability is not observed. Fig. 24 shows a simulation calculation using RELAP5/MOD3.2 code for this scheme (Vijayan et al. (2005)).

b) It is well known that the lower threshold is due to boiling inception and this instability disappears at relatively moderate pressures. Hence a start-up scheme involving a one-time pressurization to a moderate pressure followed by heat up with fission heat at low power is being investigated. Here boiling is initiated at the moderate pressure. Typical simulation of this procedure is shown in Fig. 25 at two different pressures. As expected at the higher pressure, the amplitude of oscillations observed at boiling inception is significantly low.

8.3. Power Raising Procedure

It may be noted that the stability maps were generated with the linear stability method by assuming infinitesimal disturbances to the steady state condition. However, during actual operation of a NC reactor, the power raising is in finite small steps. Experimental evidence in natural circulation loops suggests that there is a hysteresis region where the stability threshold depends on the operating procedure. Hence the proposed procedure for power raising and setback needs to be validated

experimentally. A simulation calculation for a typical power raising procedure where power is raised at the rate of 0.5% per second is given in Fig. 26a. The corresponding path traced on the stability map is shown in Fig 26b. It is found that the standard power raising procedure followed in forced circulation BWRs can be adopted without causing instability. In addition simulation calculations are required to ensure that the adopted procedures for power step back, setback, etc. do not cause entry into the unstable zone (Vijayan et al. (2005)).

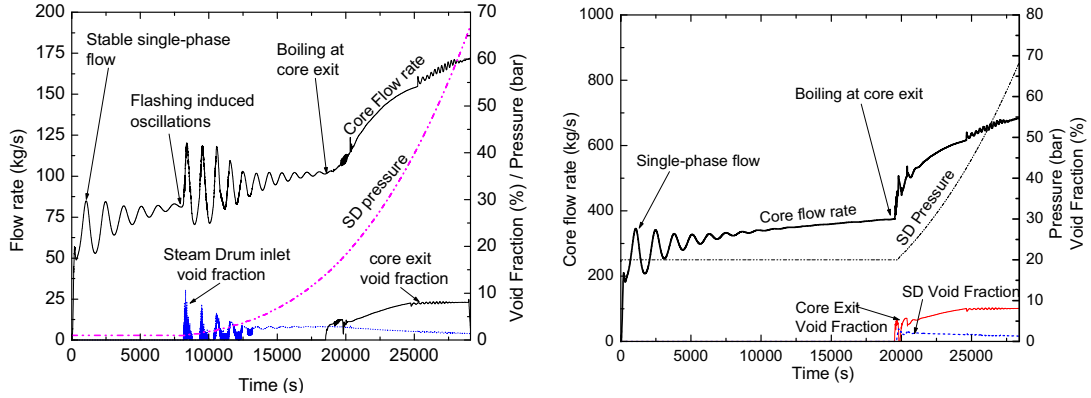

(a) Start-up at 0.1 MPa *(b) Start-up at 2 MPa*

FIG. 25. Start-up simulation at different pressures

8.4. Instability Monitoring

In spite of specifying a start-up and operating procedure, it is possible to land in the unstable zone due to a malfunction or failure of equipments such as failure of feed water heaters or control rod drives. In such cases, incorporation of auto-detect and suppress systems can help in instability control. Generally such systems rely on the decay ratio calculated on the basis of the noise analysis of measured neutron flux signals. There are recent reports, questioning the adequacy of the decay ratio in BWR stability monitoring (van der Hagen (2000)) especially in case of dual oscillations.

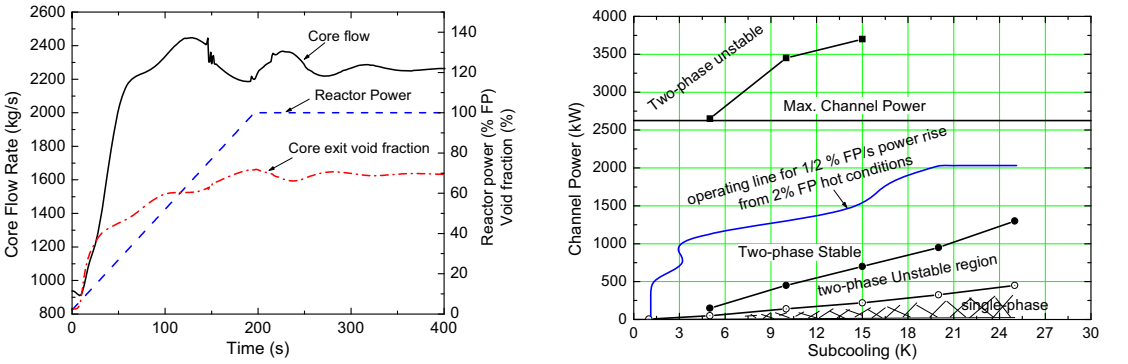

(a) Predicted power raising transient (b) Power raising procedure on the stability map

FIG.26.Simulation of power raising at 0.5% FP/s from 2% FP to 100 % FP at 7 MPa

8.5. Closure

In most cases, the parametric effects are found to exhibit the same trend as in a forced circulation BWR. Differences exist in inlet orificing due to the low value of driving force. Since decay ratio is not an established indicator of stability margin especially during the dual oscillations, the operating and start-up procedures are to be extensively investigated to ensure adequate stability. The stability analysis carried out for AHWR has shown that the reactor power is not limited by stability just as in

forced circulation boilers. Therefore, avoiding the stability only restricts the start-up and operating procedure to some extent.

9. STABILITY CONSIDERATIONS IN NC BASED SGS

Steam generator is an important component of all PWRs, PHWRs and VVERs. Most PWRs and PHWRs use vertical natural circulation U-tube steam generators whereas VVERs use horizontal steam generators. Fig. 27 shows the schematic of a vertical natural circulation U-tube steam generator. It consists of a feed water system, downcomer section, heat exchange section, top plenum with separator assembly, dryer and a steam removal system. The feed water system essentially consists of a feed water nozzle and a ring header with inverted J-tubes (not shown in Fig. 27). The subcooled feed water from the j-tubes mixes with the saturated water from the separator and flows down through the downcomer section. The heat exchange section is the tube bundle portion where the heat from the primary fluid is transferred across the tube wall to the secondary fluid causing steam generation. The steam-water separation takes place in the centrifugal separators and the separated water flows back to the downcomer whereas the steam goes through the dryer unit and exits from the SG dome. The NC flow on the secondary side takes place due to the density difference in the downcomer region and the heat exchange section. Generally, the recirculation ratio (downcomer flow/feed flow) is typically in the range of 3 to 5 at full power condition.

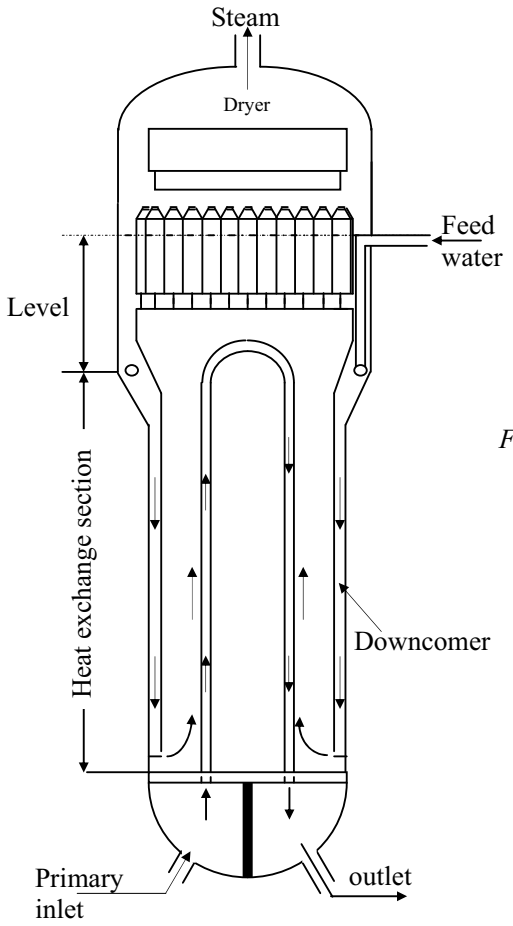

FIG..27. NC based nuclear steam generator

SGs are subject to static instability of the Ledinegg type and density wave dynamic instabilities. The stability behaviour of NC based SGs used in PWRs is rather well understood. Generally, the existing SG designs show instability only at significantly high power (> 1.5 times the nominal full power). Most of the recent studies pertain to liquid sodium cooled steam generators used in LMFBRs (Lorenzini et al. (2003), Unal et al. (1977). Most of these SGs, however, are the forced circulation type. Often the SGs used in LMFBRs are stabilized by orificing at the inlet of the tubes at the expense of enhanced pumping power. Most SGs use very long U-tubes (typically 15 to 30 m) leading to very large transit times and hence very low frequency of oscillations. Analysis of SG instability is complicated because of the coupling with the primary fluid dynamics. Both linear (STEAMFREQ-X by Chan and Yadigaroglu (1985)) and nonlinear codes (LeCoq et al. (1990)) for stability analysis of steam generators are reported in literature. Again, nonlinear analysis can be carried out with system codes and codes developed for normal transient analysis of SGs. A computer code for normal transient analysis of NC based SGs is described by Hoeld (1978).

10. CLOSING REMARKS ON THE DESIGN PROCEDURE OF NC BWRS

Stability design of NC BWRs, where several different instability mechanisms can be simultaneously acting is somewhat involved and is not well documented. The same is the case with any two-phase NC loop with several parallel channels. Strictly speaking, natural circulation systems shall be analyzed for all known instabilities. However, well-established analysis procedures do not exist for all instabilities. Ledinegg instability, flashing instability and geysering are observed only at low pressures. Pressure drop oscillations may not be important for systems without compressible volumes at the inlet. Thermal oscillations are associated with systems after dryout which can be avoided by established design procedures. Both density wave and acoustic instabilities can occur at high pressures. But density wave instability is more common. Even so, DWI can be whole loop (system instability or in-phase instability) or parallel channel instability (out-of-phase instability) and both can be neutronically coupled. For design, the first issue is which of them is controlling (i.e. having the least stable zone)? Probing calculations may be necessary to identify this. For NC BWRs, the out-of-phase oscillations can be the controlling mode as was observed in AHWR. For AHWR, a conservative stability map could be generated with the maximum rated twin channel system. The effect of a negative void coefficient was to stabilize the pure thermalhydraulic instability. Usually, DWI has a lower and an upper threshold of instability. For AHWR, the upper threshold is higher than the CHF threshold and is not expected to occur as CHF limits the power. The lower threshold can be encountered during start-up and power raising. To avoid this, a start-up procedure needs to be specified for avoiding the unstable zone. The start-up procedure also ensures that the boiling is initiated at powers above the flow reversal threshold. In spite of this, NC BWRs can land up in an unstable zone during an unanticipated operational transient. In such cases, incorporation of an auto-detect and suppress mechanism will be useful.

NOMENCLATURE

A - flow area, m^2
a_i - dimensionless flow area, A_i/A_r
b - constant in friction factor equation
C_D - Doppler coefficient ($\Delta k/k/\Delta T$)
$C_m(t)$ - delayed neutron precursor concentration of group m
Cp - specific heat, J/kgK
C_α - void reactivity coefficient ($\Delta k/k/\Delta\gamma$)
D - hydraulic diameter, m
d_i - dimensionless hydraulic diameter, D_i/D_r
f - Darcy-Weisbach friction coefficient
g - gravitational acceleration, m/s^2

Gr_m - modified Grashof number, $D^3\rho^2\beta g\Delta T_r/\mu^2$
h - enthalpy J/kg
h_{fg} - latent heat of vaporization, J/kg
H_f - heat transfer coefficient, W/m^2K
H - loop height, m
k(t) - effective multiplication factor
K - local pressure loss coefficient
k - thermal conductivity, W/mK
l - prompt neutron life time (s)
l_i - dimensionless length, L_i/L_t
L - length, m
m_f - mass of fuel rods, kg
n(t) - neutron density
N - total number of pipe segments
N_f - Froude number, $gLA\rho_f^2/W^2$
N_{fr} - friction number, fL/2D
N_p - phase change number, $Q_h\rho_f/(Wh_{fg}\rho_g)$
N_{pch} - phase change number (Q_h/Wh_{fg})
N_{sub} - subcooling number $(\Delta h_{sub}/h_{fg})$
N_s - subcooling number, $\Delta h_i\rho_f/h_{fg}\rho_g$
Nu_m - modified Nusselt number, U_iL_t/k
N_G - geometric contribution to the friction number
p - pressure, N/m^2
Pr - Prandtl number, $Cp\mu/k$
p - constant in friction factor equation
Q - total heat input rate, W
q_h - volumetric heat generation, W/m^3
Re - Reynolds number, $DW/A\mu$
S - stability parameter
S - dimensionless co-ordinate around the loop, s/H
s - co-ordinate around the loop, m
St_m - modified Stanton number, $4Nu_m/Re_{ss}Pr$
t - time, s
T - temperature, K
ΔT_r - reference temperature difference $(Q_hH/A\mu Cp)$, K
v - specific volume, m^3/kg
v_{fg} - $v_g - v_{f,m}{}^3/kg$
W - mass flow rate, kg/s
Δz - centre line elevation difference between cooler and heater, m

Greek Symbols

α - coupling coefficient
β - thermal expansion coefficient, K^{-1} and delayed neutron fraction
γ - void fraction
θ - dimensionless temperature
λ - decay constant of delayed neutron group m
μ - dynamic viscosity, Ns/m^2
ρ_0 - reference density, kg/m^3
σ - thermal expansion coefficient, K^{-1}
τ - nondimensional time, and residence time, s
τ_f - fuel time constant (s)

ϕ - dimensionless circulation length, L_t/H

ϕ_{LO}^2 - two-phase friction multiplier

ω - dimensionless mass flow rate

Subscripts

av - average
c - cooler, core
ch - channel
cl - cold leg
d - downcomer
e - equivalent
eff - effective
f - saturated liquid
g - saturated vapour
h - heater
H - header
hl - hot leg
i - i^{th} segment
in - inlet
o - outlet
r - reference value
sat - saturation
SD - steam drum
sp - single-phase
ss - steady state
ss,av- average steady state
sub - subcooling
t - total
tp - two-phase

Superscripts

‘ - perturbed

$\bar{}$ - average

REFERENCES

Achard, J-L, Drew, D.A, Lahey Jr, R.T, 1985, The analysis of nonlinear density wave oscillations in boiling channels, *Journal of Fluid Mechanics* **155**, pp.213-232.

Ambrosini, W. and Ferreri, J.C., 1998, The effect of truncation error on the numerical prediction of linear stability boundaries in a natural circulation single-phase loop, *Nuclear Engineering and Design* **181**, pp.53-76.

Aritomi, M, Aoki, S. and Inoue, A, 1986, Thermo-hydraulic instabilities in parallel boiling channel systems Part 1. A non-linear and a linear analytical model, *Nuclear Engineering and Design* **95**, pp.105-116.

Baroczy, C.J., 1966, A systematic correlation for two-phase flow pressure drop, *Chem. Eng. Progr. Symp. Ser.* **62**, pp.232-249.

Barre, F, Dor, I, and Brun, B., 1993, Advanced numerical methods for thermalhydraulics, *Nuclear Engineering Design,* **145**, pp.147-158.

Beuthe, T.G. and Hanna, B.N., 2005, CATHENA MOD-3.5d Theory Manual, 153-112020-STM-001, Revision 0, December 2005.

Chan, K.C, 1989, FABLE02V User's Manual, NEDE-31732P.

Chan, K.C. and Yadigaroglu, G, 1986, Analysis of density wave instability in counterflow steam generators using STEAMFREQ-X, *Nuclear Engineering and Design* **93**, pp.15-24.

Chang Chin-Jang and Lahey Jr. R.T., 1997, Analysis of chaotic instabilities in boiling systems, *Nuclear Engineering and Design* **167**, pp.307-334.

Chato, J.C., 1963, Natural convection flows in a parallel channel system, *J. Heat Transfer* **85**, pp.339-345.

Chatoorgoon, V, 1986, SPORTS – a simple nonlinear thermal-hydraulic stability code, *Nuclear Engineering Design,* **93**, pp.51-67.

Chen, W.L, Wang, S.B, Twu, S.S, Chung, C.R. and Chin Pan, 2001, Hysteresis effect in a double channel natural circulation loop, *International Journal of Multiphase Flow,* **27,** pp.171-187.

Creveling, H.F. De Paz, J.Y. Baladi and R.J. Schoenhals, 1975, Stability characteristics of a single-phase free convection loop, *J. Fluid Mech.* **67**, pp.65-84.

D'Auria, F. et al., 1997, State of the Art Report on Boiling Water Reactor Stability, OCDE/GD(97)13, OECD-NEA.

Dimmick, G.R, Chatoorgoon, V, Khartabil, H.F. and Duffey, R.B., 2002, Natural convection studies for advanced CANDU reactor concepts, *Nuclear Engineering and Design* **215**, pp.27-38.

Ferreri J.C, Ambrosini, W., 2002, On the analysis of thermal-fluid-dynamic instabilities via numerical discretization of conservation equations, *Nuclear Engineering and Design,* **215**, pp.153–170.

Fletcher, C.D. and Schultz R.R., 1995, RELAP5/MOD3 Code Manual, NUREG/CR-5535, INEL, Idaho Falls, Idaho.

Hănggi, P., 2001, Investigating BWR Stability with a New Linear Frequency-Domain Method and Detailed 3D Neutronics, Ph.D Thesis, Swiss Federal Institute of Technology, Zurich

Hoeld, A, 1978, A theoretical model for the calculation of large transients in nuclear natural circulation U-tube steam generators (Digital code UTSG), *Nuclear Engineering and Design* **47**, pp.1-23.

Lahey, Jr, R.T, Engineering applications of fractal and chaos theory in Modern developments in multiphase flow & heat transfer, *Center for Multiphase Research,* Rensselaer Polytechnic Institute, Troy, NY - USA 12180-3590.

LeCoq, G, Metaich, M. and Slassi-Sennou, 1990, A simple model for the study of dynamic instabilities in steam generators, *Nuclear Engineering and Design,* **122**, pp.41-52.

Lerchl, G. and Austregesilo, H, 2000, ATHLET Mod 1.2 Cycle C: User's Manual, Gesellschaft für Anlagen und Reaktorsicherheit (GRS) mbH, Nov. 2000.

Linzer, W and Walter, H, 2003, Flow reversal in natural circulation systems, *Applied Thermal Engineering,* **23**, pp.2363-2372.

Lorenzini, E. Spiga, M. Iadarola G. and D'Auria F., 1991, Density wave instabilities in steam generators, *Annals of Nuclear Energy,* **18**, pp.31-42.

Manish Sharma, P.K. Vijayan, A.K. Nayak, D. Saha and R.K. Sinha, 2002, Numerical study of stability behaviour of single-phase natural circulation in a rectangular loop, *Proceedings of 5th ISHMT-ASME Heat and Mass Transfer Conference,* Kolkata, India Jan. 3-5, pp. 1204-1210.

Manish Sharma, D.S. Pilkhwal, P.K. Vijayan, D. Saha and R.K. Sinha, 2002, Single-phase instability behaviour in a rectangular natural circulation loop using RELAP5/MOD3.2 computer code, BARC/2002/E/012.

Manish Sharma, D.S. Pilkhwal, P.K. Vijayan, D. Saha and R.K. Sinha, 2004, Simulation of single-phase instability behaviour in a rectangular natural circulation loop, HMT-2004-C028, *Proceedings of 6th ISHMT-ASME Heat and Mass Transfer Conference,* Kalpakkam, India, Jan. 5-7.

Maqua, M, Kotthoff, K and Pointner, W, Neutron flux oscillations at German PWRs, GRS Technical Report.

March-Leuba, J. 2000, Review of the STAIF/MICROBURN-2 BWR Stability Analysis Methodology, Technical Evaluation Report ORNL/NRC/LTR-00/05, June 2000.

Misale, M. and Frogheri, M., 1999, Influence of pressure drops on the behaviour of a single-phase natural circulation loop: Preliminary results, *Int. Comm. Heat Mass Transfer* **26**, pp.597-606.

Misale, M, Frogheri, M, D'Auria, F. and Fontani, E. and Garcia, A., 1999, Analysis of single-phase natural circulation experiments, International *Journal of Thermal Sciences,* **38**, pp.977-983.

Muñoz-Cobo, J.L. García, C. Escrivá A. and José Melara, 2006, 1 D Neutronic model in the frequency domain and its coupling to the stability code LAPUR, Top_Fuel 2006, International meeting on LWR fuel performance "nuclear fuel: addressing the future" 22-26 October 2006 Salamanca, Spain

Nayak, A.K, Vijayan, P.K, Saha, D, Venkat Raj, V. and Aritomi M, 1998, Linear analysis of thermo-hydraulic instabilities of the Advanced Heavy Water Reactor (AHWR), *Journal of Nuclear Science and Technology,* **35**, pp.768-778.

Nayak, A.K, Vijayan, P.K, Saha, D, Venkat Raj, V. and Aritomi, M, 2000a, Analytical study of nuclear-coupled density-wave instability in a natural circulation pressure tube type Boiling Water Reactor, *Nuclear Engineering and Design* **195**, pp.27-44.

Nayak, A.K, Vijayan P.K, and Saha, D, 2000b, "Analytical modelling and study of the stability characteristics of the Advanced Heavy Water Reactor", BARC/2000/E/011.

Nayak, A.K, Vijayan, P.K, Saha, D, Venkat Raj, V, and Aritomi, M., 2002, Study on the stability behaviour of a natural circulation pressure tube type boiling water reactor, *Nuclear Engineering and Design* **215**, pp.127-137.

Nishina, K. and Tokashiki, M., 1996, Verification of more general correspondence between the eigen value separation and coupling coefficient, *Ann. Nucl. Energy,* **30,** pp.277-286.

Otaudy, P. and March-Leuba, J., 1989, LAPUR User's Guide, NUREG/CR-5421.

Paulsen, M.P., McFadden, J.H., Peterson, C.E., McLure, J.A., Gose, G.C. and Jensen, P.J., 1991, The RETRAN-03 Computer Code, *Nuclear Technology,* **95**, pp.105-115.

Pazsit, I., 1995, Determination of reactor stability in case of dual oscillations, *Ann. Nucl. Energy,* **22**, pp.377-387.

Peng, S.J, Podowski, M.Z, and Lahey, Jr., R.T, 1985, NUFREQ-NP: A digital computer code for the linear stability analysis of boiling water nuclear reactors, NUREG/CR-4116.

RELAP5 development team, 1995, RELAP5/MOD3.2 Code Manual, Volume I: Code structure, system models, and solution methods, NUREG/CR-5535 or INEL-95/0174, Idaho National Engineering Laboratory, Lockheed Idaho Technologies Company, Idaho Falls, Idaho 83415.

Rohatgi, U.S. and Duffey, R.B., 1998, Stability, DNB, and CHF in natural circulation two-phase flow, *Int. Comm. Heat Mass Transfer,* **25**, pp.161-174.

Sanders, J, 1988, Stability of single-phase natural circulation with inverted U-tube steam generators, *J. Heat Transfer,* **110**, pp.735-742.

Song, J.H, and Ishii, M., 2001, On the stability of a one-dimensional two-fluid model, *Nuclear Engineering and Design,* **204**, pp.101-115.

Stenning, A.H. and Veziroğlu, T.N, 1965, Flow oscillation modes in Forced-Convection Boiling, *Proc. 1965 Heat Transfer and Fluid Mechanics Inst.,* pp. 301-316, Stanford University Press, Stanford, Calif..

Takeuchi, Y., Uematsu, H., Ebata, S., Shaug, J.C., Shiralkar, B.S., 1994, TRACG Transient Analysis Code, Three Dimensional Kinetics Model Implementation and Applicability or Space Dependent analysis, *Nucl. Technol.* **105**.

Turso, J.A, March-Leuba, J, Edwards, R.M, 1997, A modal reduced order model of BWR out-of-phase instabilities, *Ann. Nucl. Energy,* **24**, pp.921-934.

Ünal H. C. van Gasselt M. L. G. and Ludwig, P. W. P. H, 1977, Dynamic instabilities in tubes of a large capacity, straight-tube, once-through sodium heated steam generator, *International Journal of Heat and Mass Transfer,* **20**, pp.1389-1399.

van der Hagen T.H.J.J, Pazsit, I, Thomson O and Melkerson B, 1994, *Nuclear Technology,* **107**, pp.193-217.

van der Hagen T.H.J.J, Zboray, R. and de Kruijif, W.J.M, 2000, Questioning the use of decay ratio in BWR stability monitoring, *Annals of Nuclear Energy* **27,** pp.727-732.

Vijayan, P.K, Venkat Raj, V, Nagdaune R.K and Pilkhwal, D.S., 1991, Thermosyphon tests and comparison with code predictions for a PHWR, *3rd International Seminar on small and medium sized reactors,* New Delhi, August 26-28.

Vijayan P.K. and Austregesilo, H., 1994, 'Scaling laws for single-phase natural circulation loops', *Nuclear Engineering Design,* **152**, pp.331-334.

Vijayan, P.K. Austregesilo H. and Teschendorff V. 1995, 'Simulation of the unstable oscillatory behaviour of single-phase natural circulation with repetitive flow reversals in a rectangular loop using the computer code ATHLET', *Nuclear Engineering Design* **155**, pp.623-641.

Vijayan, P.K. Bhojwani, V.K. Bade, M.H. Sharma, M. Nayak, A.K. Saha D. and Sinha, R.K., 2001, Investigations on the effect of heater and cooler orientation on the steady state, transient and stability behaviour of single-phase natural circulation in a rectangular loop, BARC/2001/E/034.

Vijayan, P.K, 2002, Experimental observations on the general trends of the steady state and stability behaviour of single-phase natural circulation loops, *Nuclear Engineering and Design* **215**, pp.139-152.

Vijayan, P.K., Bade M.H, Saha D, Sinha, R.K, and Venkat Raj V. A, 2004a, Generalized Flow Correlation for Single-Phase Natural Circulation Loops**,** *Proceedings of 6th ISHMT-ASME Heat and Mass Transfer Conference,* Kalpakkam, Jan. 5-7, HMT-2004-C022.

Vijayan, P.K., Manish Sharma, Pilkhwal, D.S. Saha D, Sinha, R.K, Bhojwani V.K. and Sane N. K., 2004b, Experimental and numerical investigations on the nature of the unstable oscillatory flow in a single-phase natural circulation loop, *Proceedings of 6th ISHMT-ASME Heat and Mass Transfer Conference*, Kalpakkam, Jan. 5-7, 2004b, HMT-2004-C100.

Vijayan, P.K, Nayak, A.K, Rao, G.S.S.P., Bagul, R.K., Saha, D. and Sinha, R.K. 2005, Designing for stability in a natural circulation pressure tube type boiling water reactor, The 11th International Topical Meeting on Nuclear Reactor Thermal-Hydraulics (NURETH-11), Paper: 154, Popes' Palace Conference Center, Avignon, France, October 2-6, 2005.

Vijayan, P.K. Sharma M. and Saha, D. 2007, Steady state and stability characteristics of single-phase natural circulation in a rectangular loop with different heater and cooler orientations, Experimental Thermal and Fluid Science 31, 925-945.

Welander, P, 1967, On the oscillatory instability of a differentially heated loop, *J. Fluid Mech.* **29**, pp.17-30.

Zerreßen, K.W., Kreuter, D, 1987, Post-calculation of core instabilities measured in the German BWRs KRB-B/C Using the frequency domain code STAIF, *International workshop on abnormal transients in nuclear power plants*, Atlanta.

Zhou, J. and Podowski, M.Z., 2001, Modeling and analysis of hydrodynamic instabilities in two-phase flow using two-fluid model, *Nuclear Engineering and Design* **204**, pp.129-142.

Zuber, N, 1966, An analysis of thermally induced flow oscillations in the near critical and supercritical thermodynamic region, NAS 8-11422, final report.

APPENDIX-1: Brief description of AHWR

The Advanced Heavy Water Reactor being designed by India is a vertical pressure tube type heavy water moderated light water cooled BWR. It uses dual MOX fuel consisting of plutonium, thorium and U-233. Fig.A-1.1 shows a schematic of the AHWR primary circuit. Two-phase circulation is chosen as the mode of primary coolant circulation. To achieve the desired circulation rate, the steam drum is elevated. Total height of the loop is typically 40 m. The main components of the loop are the steam drum and the core. There are four steam drums (3.75 m inside diameter) connected to a common inlet header (600 mm NB) through 16 downcomers (300 mm NB and four from each steam drum). From the header 452 inlet feeders (100 mm NB) connect to an equal number of pressure tubes and joins the steam drum through an equal number of tail pipes (125 mm NB). The pressure tube inside diameter is 120 mm and it houses a 54-rod bundle with an active core height of 3.5 m. Under normal operation a level is maintained in the steam drum. The steam pressure is maintained at 7 MPa.

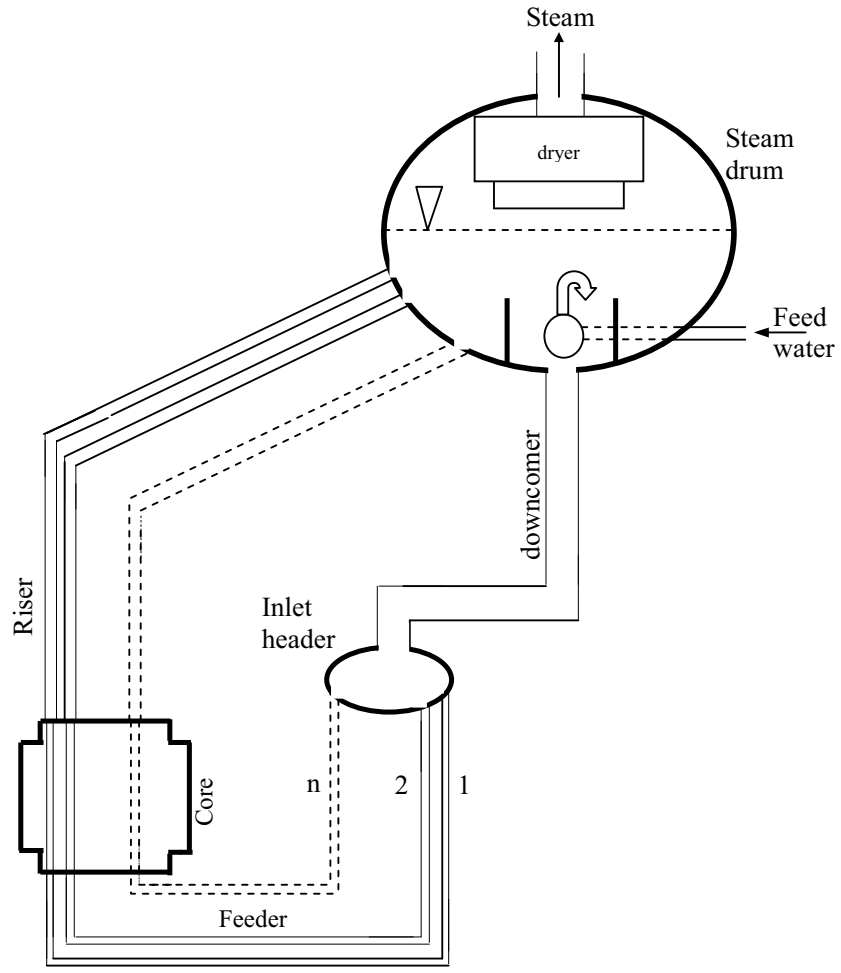

FIG. A-1.1: Schematic of AHWR system

APPENDIX-2: STEADY STATE FLOW FOR SINGLE-PHASE NC

The governing equations in terms of the mass flow rate and cross-sectional average temperature for 1-dimensional incompressible single-phase natural circulation flow in a closed loop such as Fig. 4, can be written as

$$\frac{\partial W}{\partial s} = 0 \tag{A-2.1}$$

$$\frac{L_t}{A}\frac{dW}{dt} = g\oint \rho dz - \frac{f\left(L_{eff}\right)_t W^2}{2D\rho_0 A^2} \tag{A-2.2}$$

where $(L_{eff})_t$ is the effective length taking into account the local losses. If the local losses are negligible, then $(L_{eff})_t$ is the loop circulation length, L_t

$$\frac{\partial T}{\partial t} + \frac{W}{A\rho_0}\frac{\partial T}{\partial s} = \begin{Bmatrix} \dfrac{4q}{D\rho_0 Cp} \quad heater \quad \left(for \quad 0 < s \le s_h\right) \\ 0 \quad pipes \quad \left(for \quad s_h < s \le s_{hl} \quad and \quad s_c < s \le L_t\right) \\ -\dfrac{4U}{D\rho_0 Cp}\left(T - T_s\right) \quad cooler \quad \left(for \quad s_{hl} < s \le s_c\right) \end{Bmatrix} \tag{A-2.3}$$

The energy equation neglects the effect of axial conduction and viscous dissipation. The above equations are nondimensionalized with the following substitutions:

$$\omega = \frac{W}{W_{ss}};\ \theta = \frac{T - T_s}{\left(\Delta T_h\right)_{ss}};\ \tau = \frac{t}{t_r};\ S = \frac{s}{H}\ and\ Z = \frac{z}{H} \tag{A-2.4}$$

Where $t_r = V_t\rho_0/W_{ss}$. Utilizing the Boussinesq approximation and nondimensionalizing the momentum and energy equations assuming negligible local pressure losses, we get

$$\frac{d\omega}{d\tau} = \frac{Gr_m}{\mathrm{Re}_{ss}^3}\oint \theta\, dZ - \frac{pL_t\omega^{2-b}}{2D\,\mathrm{Re}_{ss}^b} \tag{A-2.5}$$

$$\frac{\partial\theta}{\partial\tau} + \phi\omega\frac{\partial\theta}{\partial S} = \begin{Bmatrix} \dfrac{L_t}{L_h}\ for\ 0 < S \le S_h\ heater \\ 0\ for\ S_h < S \le S_{hl}\ and\ S_c < S \le S_t\ \ pipes \\ -St_m\theta\ for\ S_{hl} < S \le S_c\ cooler \end{Bmatrix} \tag{A-2.6}$$

Where ϕ is a non-dimensional parameter given by $\phi = L_t / H$. The steady state solution for the momentum and energy equations can be obtained by setting $\omega_{ss} = 1$ and $\partial\omega/\partial\tau = \partial\theta/\partial\tau = 0$. The solution of the energy equation for the various segments of the loop can be written as

$$\theta = \theta_{cl} + \tfrac{H}{L_h}S \qquad \text{Heater } (0<S\le S_h) \tag{A-2.7a}$$

Where the boundary condition that at S=0, $\theta = \theta_{cl}$ has been used. Similarly for the hot leg (by setting $S=S_h$ in the above equation) we get

$$\theta = \theta_{cl} + 1 = \theta_{hl} \qquad \text{Hot leg } (S_h < S \leq S_{hl}) \qquad \text{(A-2.7b)}$$

For the cooler we get

$$\theta = \theta_{hl} e^{\frac{St_m}{\phi}(S_{hl} - S)} \qquad \text{Cooler } (S_{hl} < S \leq S_c) \qquad \text{(A-2.7c)}$$

Where the boundary condition that at $S=S_{hl}$, $\theta = \theta_{hl}$ has been used. For the cold leg using the boundary condition that at $S=S_c$, $\theta = \theta_{cl}$ we get

$$\theta = \theta_{hl} e^{\frac{-St_m L_c}{L_t}} = \theta_{cl} \qquad \text{Cold leg } (S_c < S \leq S_t) \qquad \text{(A-2.7d)}$$

From the above equations explicit expressions for the cold leg and hot leg temperatures can be obtained as

$$\theta_{cl} = \frac{1}{e^{\frac{St_m L_c}{L_t}} - 1} \qquad \text{(A-2.8a)}$$

$$\theta_{hl} = \frac{1}{1 - e^{-St_m \frac{L_c}{L_t}}} \qquad \text{(A-2.8b)}$$

The steady state solution of the momentum equation can be written as

$$\mathrm{Re}_{ss} = \left[\frac{2}{p} Gr_m \frac{D}{L_t} I_{ss} \right]^{\frac{1}{3-b}} \qquad \text{(A-2.9)}$$

Where $I_{ss} = \oint \theta_{ss} dZ$. Using Eq. (A-2.7), expressions for I_{ss} for the different orientations of the heater and cooler can be derived. Even for the same orientation, the numerical value of the integral is different for the clockwise and anticlockwise flow. Steady flow in both the clockwise and anticlockwise directions is possible only with horizontal heaters. For the HHHC orientation, however, the integral is the same for both flow directions. Therefore, the integral is evaluated for both flow directions for the HHVC orientation only.

HHHC Orientation

The geometry and coordinate system adopted is shown in Fig. A-2.1. L_1, L_2, L_3 and L_4 are the lengths of the respective horizontal unheated sections in the figure. L_h, L_{hl}, L_c and L_{cl} are respectively the lengths of the heater, hot leg, cooler and cold leg. The pipe between end of the heated section and the beginning of the cooled section is the hot leg. Similarly, the pipe between the end of the cooler and the beginning of the heater is the cold leg. The nondimensional lengths S_h, S_{hl}, S_c and S_t are the cumulative distances from the origin, which is taken as the beginning of the heated section. The nondimensional length S_1, S_2, S_3 and S_4 are the cumulative distances from the origin to the four corners of the rectangular loop.

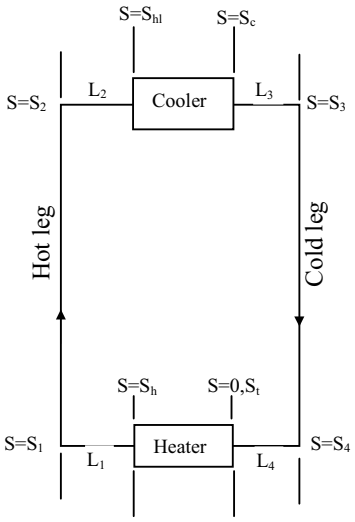

FIG. A-2.1. Loop Geometry and co-ordinates for the HHHC orientation

Since dZ=0 for horizontal sections, the integral in the momentum equation can be written as

$$I_{ss} = \oint [\theta(S)]_{ss}\, dZ = \int_{S_1}^{S_2} (\theta_{hl})_{ss}\, dZ + \int_{S_3}^{S_4} (\theta_{cl})_{ss}\, dZ \qquad \text{(A-2.10)}$$

For the up leg dZ=dS and for the down leg dZ = -dS. Also, $S_2 = S_1+1$ and $S_4=S_3+1$ since lengths are nondimensionalised using H (i.e. loop height). Hence

$$\oint [\theta(S)]_{ss}\, dZ = \int_{S_1}^{S_1+1} (\theta_{hl})_{ss}\, dS - \int_{S_3}^{S_3+1} (\theta_{cl})_{ss}\, dS \qquad \text{(A-2.11)}$$

Which can be written as

$$\oint [\theta(S)]_{ss}\, dZ = (\theta_{hl})_{ss} - (\theta_{cl})_{ss} \qquad \text{(A-2.12)}$$

From equation (A-2.7b) we obtain $(\theta_{hl})_{ss} - (\theta_{cl})_{ss} = 1$. Therefore, for the HHHC orientation we get

$$I_{ss} = \oint [\theta(S)]_{ss}\, dZ = 1 \qquad \text{(A-2.13)}$$

<u>H</u>HVC Orientation

The geometry and co-ordinate system adopted for the HHVC orientation is given in Fig. A-2.2. The integral can be evaluated as

$$I_{ss} = \int_{S_1}^{S_1+1} (\theta_{hl})_{ss}\, dS - \int_{S_3}^{S_{hl}} (\theta_{hl})_{ss}\, dS - \int_{S_{hl}}^{S_c} (\theta_{hl})_{ss}\, e^{\frac{St_m}{\phi}(S_{hl}-S)}\, dS - \int_{S_c}^{S_4} (\theta_{cl})_{ss}\, dS \qquad \text{(A-2.14)}$$

After integrating and substituting the limits we get

$$I_{ss} = (\theta_{hl})_{ss} - (\theta_{hl})_{ss}\frac{L_2}{H} + (\theta_{hl})_{ss}\frac{\phi}{St_m}\left[e^{\frac{-St_m L_c}{L_t}} - 1\right] - (\theta_{cl})_{ss}\frac{L_3}{H} \quad \text{(A-2.15)}$$

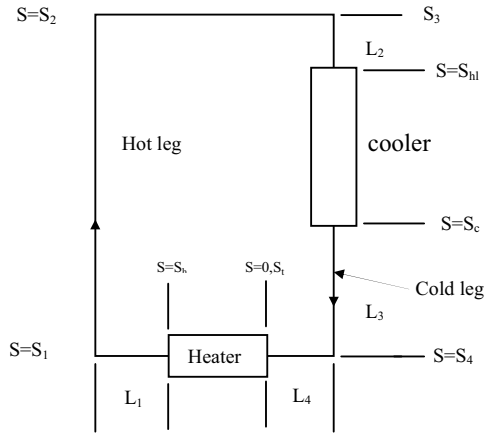

FIG. A-2.2. Loop Geometry and co-ordinates for the HHVC orientation

Noting that $\theta_{hl} = \theta_{cl}+1$ and using equations (A-2.8a) and (A-2.8b) we get

$$I_{ss} = \frac{H - L_2 - L_3}{H\left(e^{\frac{St_m L_c}{L_t}} - 1\right)} + \left(1 - \frac{L_2}{H}\right) - \frac{L_t}{St_m H}$$

The integral can be evaluated as

$$I_{ss} = \int_{S_1}^{S_1+1}(\theta_{hl})_{ss}\,dS - \int_{S_3}^{S_{hl}}(\theta_{hl})_{ss}\,dS - \int_{S_{hl}}^{S_c}(\theta_{hl})_{ss}\,e^{\frac{St_m}{\phi}(S_{hl}-S)}\,dS - \int_{S_c}^{S_4}(\theta_{cl})_{ss}\,dS \quad \text{(A-2.14)}$$

After integrating and substituting the limits we get

$$I_{ss} = (\theta_{hl})_{ss} - (\theta_{hl})_{ss}\frac{L_2}{H} + (\theta_{hl})_{ss}\frac{\phi}{St_m}\left[e^{\frac{-St_m L_c}{L_t}} - 1\right] - (\theta_{cl})_{ss}\frac{L_3}{H} \quad \text{(A-2.15)}$$

Noting that $\theta_{hl} = \theta_{cl}+1$ and using equations (A-2.8a) and (A-2.8b) we get

$$I_{ss} = \frac{H - L_2 - L_3}{H\left(e^{\frac{St_m L_c}{L_t}} - 1\right)} + \left(1 - \frac{L_2}{H}\right) - \frac{L_t}{St_m H} \quad \text{(A-2.16)}$$

Since $L_c = (H-L_2-L_3)$, we obtain

$$I_{ss} = \frac{L_c}{H}\left[1 + \frac{1}{e^{\frac{St_m L_c}{L_t}} - 1}\right] + \frac{L_3}{H} - \frac{L_t}{St_m H} = \frac{L_c}{H}\left[\frac{1}{1 - e^{\frac{-St_m L_c}{L_t}}}\right] + \frac{L_3}{H} - \frac{L_t}{St_m H} \quad \text{(A-2.17)}$$

VHHC Orientation

The loop geometry and co-ordinate system for this case is shown in Fig. A-2.3. The integral in the momentum equation can be written as

$$I_{ss} = \int_0^{S_h}\left((\theta_{cl})_{ss} + \frac{H}{L_h} S \right) dS + \int_{S_h}^{S_2} (\theta_{hl})_{ss}\, dS - \int_{S_3}^{S_4} (\theta_{cl})_{ss}\, dS + \int_{S_1}^{S_t} (\theta_{cl})_{ss}\, dS \qquad \text{(A-2.18)}$$

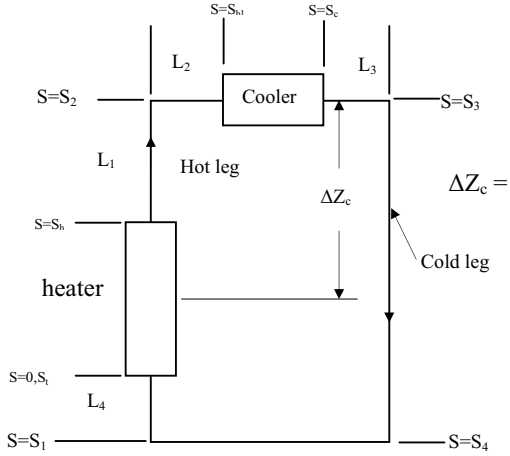

$\Delta Z_c = 0.5L_h + L_1$ = Centre line elevation difference between the cooler and the heater

FIG.. A-2.3. Loop Geometry and co-ordinates for the VHHC orientation

Integration of Equation (A-2.18) and substituting the limits yields

$$I_{ss} = (\theta_{cl})_{ss}\left(\frac{L_h}{H} - 1 + \frac{L_4}{H} + \frac{L_1}{H} \right) + \frac{L_h}{2H} + \frac{L_1}{H} \qquad \text{(A-2.19)}$$

Where $(\theta_{hl})_{ss} = (\theta_{cl})_{ss}+1$ has been used. Noting that $H=L_h+L_1+L_4$ we obtain

$$I_{ss} = \frac{L_1 + 0.5L_h}{H} = \frac{\Delta Z_c}{H} \qquad \text{(A-2.20)}$$

VHVC Orientation

The loop geometry and co-ordinate system for this case is shown in Fig. A-2.4. The integral in the momentum equation can be written as

$$I_{ss} = \int_0^{S_h}\left((\theta_{cl})_{ss} + \frac{H}{L_h} S \right) dS + \int_{S_h}^{S_2} (\theta_{hl})_{ss}\, dS - \int_{S_3}^{S_{hl}} (\theta_{hl})_{ss} dS - \int_{S_{hl}}^{S_c} (\theta_{hl})_{ss}\, e^{\frac{St_m (S_{hl}-S)}{\phi}} dS - \int_{S_c}^{S_4} (\theta_{cl})_{ss}\, dS + \int_{S_1}^{S_t} (\theta_{cl})_{ss}\, dS \qquad \text{(A-2.21)}$$

Which on integration and substitution of the limits leads to

$$I_{ss} = (\theta_{cl})_{ss}\left(\frac{L_h}{H} - \frac{L_3}{H} + \frac{L_4}{H} \right) + \frac{L_h}{2H} + (\theta_{hl})_{ss}\left(\frac{L_1}{H} - \frac{L_2}{H} \right) + \frac{\phi}{St_m}\left(\frac{e^{\frac{-St_m L_c}{L_t}} - 1}{1 - e^{\frac{-St_m L_c}{L_t}}} \right) \qquad \text{(A-2.22)}$$

Where Eq. (A-2.8b) has been used. Noting that $\theta_{hl} = \theta_{cl}+1$, we obtain

$$I_{ss} = \left(\theta_{cl}\right)_{ss}\left[\frac{L_h + L_1 + L_4}{H} - \frac{L_3 + L_2}{H}\right] + \frac{0.5L_h + L_1 - L_2 - L_t / St_m}{H} \quad \text{(A-2.23)}$$

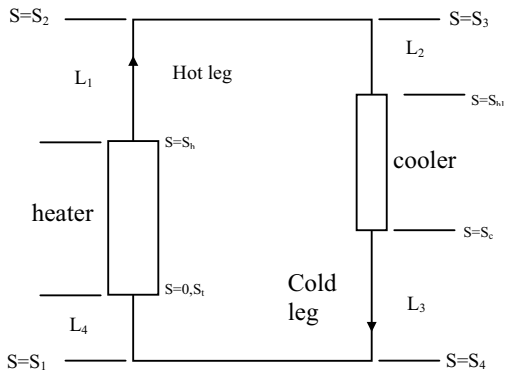

FIG.. A-2.4. Loop geometry and coordinates for VHVC orientation

which can be rewritten as

$$I_{ss} = \left[\theta_{cl}\right]_{ss}\left[1 - \left(\frac{L_3 + L_2}{H}\right)\right] + \frac{0.5L_h + L_1 - L_2 - L_t / St_m}{H} \quad \text{(A-2.24)}$$

Replacing $(\theta_{cl})_{ss}$ using (Eq. A-2.8a) and noting that L_c=H-L_3-L_2 we get

$$I_{ss} = \frac{L_c}{H\left(e^{\frac{St_m L_c}{L_t}} - 1\right)} + \frac{0.5L_h + L_1 - L_2 - L_t / St_m}{H} \quad \text{(A-2.25)}$$

HHVC Orientation with anticlockwise flow

The geometry and coordinates with this flow direction are given in Fig. A-2.5.

$$I_{ss} = \oint\left[\theta(S)\right]_{ss} dZ = \int_{S_1}^{S_{hl}}\left(\theta_{hl}\right)_{ss} dS + \int_{S_{hl}}^{S_2}\left(\theta_{hl}\right)_{ss} e^{\frac{St_m\left(S_{hl}-S\right)}{\phi}} dS + \int_{S_c}^{S_2}\left(\theta_{cl}\right)_{ss} dS - \int_{S_3}^{S_4}\left(\theta_{cl}\right)_{ss} dS \quad \text{(A-2.26)}$$

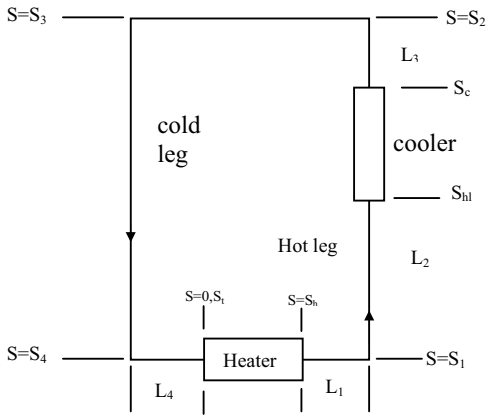

FIG.. A-2.5. Loop Geometry and co-ordinates for the HHVC orientation with flow in the anticlockwise direction

Upon integration and substituting the limits we get

$$I_{ss} = (\theta_{hl})_{ss} \frac{L_2}{H} + \frac{\phi}{St_m}(\theta_{hl})_{ss}\left(1 - e^{\frac{-St_m L_c}{L_t}}\right) + (\theta_{cl})_{ss}\left(\frac{L_3}{H} - 1\right) \quad \text{(A-2.27)}$$

Noting that H-(L_3+L_2) =L_c and using equations (A-2.8b) and (A-2.7b) we get

$$I_{ss} = -(\theta_{cl})_{ss}\left(\frac{H - L_2 - L_3}{H}\right) + \frac{L_2}{H} + \frac{L_t}{HSt_m} \quad \text{(A-2.28)}$$

which can be rearranged as

$$I_{ss} = \left(\frac{1}{1 - e^{\frac{St_m L_c}{L_t}}}\right)\left(\frac{L_c}{H}\right) + \frac{L_2}{H} + \frac{L_t}{HSt_m} \quad \text{(A-2.29)}$$

APPENDIX-3: Linear Stability analysis of single-phase NC

For uniform diameter loops with negligible local pressure losses the governing momentum and energy conservation equations in nondimensional form can be expressed as

$$\frac{d\omega}{d\tau} = \frac{Gr_m}{\mathrm{Re}_{ss}^3}\oint \theta\, dZ - \frac{pL_t\omega^{2-b}}{2D\,\mathrm{Re}_{ss}^b} \tag{A-3.1}$$

$$\frac{\partial\theta}{\partial\tau} + \phi\omega\frac{\partial\theta}{\partial S} = \begin{Bmatrix} \dfrac{L_t}{L_h} \quad heater & \left(for \quad 0 < S \le S_h\right) \\ 0 \quad pipes \quad \left(for \quad S_h < S \le S_{hl} \quad and \quad S_c < S \le S_t\right) & \\ -St_m\theta \quad cooler & \left(for \quad S_{hl} < S \le S_c\right) \end{Bmatrix} \tag{A-3.2}$$

Where ϕ is a non-dimensional parameter given by $\phi = L_t / H$. The steady state solution for the momentum and energy equations can be obtained by setting $\omega_{ss} = 1$ and $\partial\omega/\partial\tau = \partial\theta/\partial\tau = 0$. The steady state solutions for a rectangular uniform diameter loop are described in Appendix-2 for the various orientations of the heater and cooler. The stability analysis is performed by perturbing θ and ω as

$$\theta = \theta_{ss} + \theta' \; and \; \omega = \omega_{ss} + \omega' \tag{A-3.3}$$

Where θ' and ω' are small perturbations over the steady state values. With these substitutions, the perturbed momentum equation can be written as

$$\frac{d\omega'}{d\tau} = \frac{Gr_m}{\mathrm{Re}_{ss}^3}\oint \theta'\, dZ - \frac{pL_t(2-b)\omega'}{2D\,\mathrm{Re}_{ss}^b} \tag{A-3.4}$$

Where $\left(\omega_{ss} + \omega'\right)^{2-b} = \left(1 + \omega'\right)^{2-b}$ and was replaced by 1+(2-b)ω' which is valid for small values of ω' (from binomial theorem neglecting the higher order terms). The perturbed energy equation for the various segments of the loop becomes

$$\frac{\partial\theta'}{\partial\tau} + \phi\frac{\partial\theta'}{\partial S} + \frac{L_t}{L_h}\omega' = 0 \qquad \text{Heater } (0<S\le S_h) \tag{A-3.5a}$$

$$\frac{\partial\theta'}{\partial\tau} + \phi\frac{\partial\theta'}{\partial S} = 0 \qquad \text{Pipes } (S_h<S\le S_{hl} \text{ and } S_c<S\le S_t) \tag{A-3.5b}$$

$$\frac{\partial\theta'}{\partial\tau} + \phi\frac{\partial\theta'}{\partial S} + St_m\left(\theta' - \omega'\theta_{ss}\right) = 0 \qquad \text{Cooler}(S_{hl}<S\le S_c) \tag{A-3.5c}$$

The small perturbations ω' and θ' can be expressed as

$$\omega' = \bar{\omega}\varepsilon e^{n\tau} \text{ and } \theta' = \bar{\theta}(S)\varepsilon e^{n\tau} \tag{A-3.6}$$

Where ε is a small quantity and n is the stability parameter so that $\partial\theta'/\partial\tau = \bar{\theta}(S)n\varepsilon e^{n\tau}$, $\partial\theta'/\partial S = \varepsilon e^{n\tau}\partial\bar{\theta}(S)/\partial S$ and $d\omega'/d\tau = \bar{\omega}n\varepsilon e^{n\tau}$. Using these in equation (A-3.4) and (A-3.5) we get

$$n\bar{\omega} - \frac{Gr_m}{\mathrm{Re}_{ss}^3}\oint\bar{\theta}(S)\,dZ + \frac{pL_t(2-b)\bar{\omega}}{2D\,\mathrm{Re}_{ss}^b} = 0 \tag{A-3.7a}$$

which can be rewritten as

$$n - \frac{Gr_m}{\mathrm{Re}_{ss}^3}\frac{\bar{I}}{\bar{\omega}} + \frac{pL_t(2-b)}{2D\,\mathrm{Re}_{ss}^b} = 0 \tag{A-3.7b}$$

Where $\bar{I} = \oint\bar{\theta}(S)dZ.$

$$\frac{d\bar{\theta}(S)}{dS} + \frac{n}{\phi}\bar{\theta}(S) + \frac{L_t\bar{\omega}}{\phi L_h} = 0 \qquad \text{heater } (0<S\leq S_h) \tag{A-3.8a}$$

$$\frac{d\bar{\theta}(S)}{dS} + \frac{n}{\phi}\bar{\theta}(S) = 0 \qquad \text{pipes } (S_h<S\leq S_{hl} \text{ and } S_c<S\leq S_t) \tag{A-3.8b}$$

$$\frac{d\bar{\theta}(S)}{dS} + \left(\frac{n+St_m}{\phi}\right)\bar{\theta}(S) - \frac{St_m\theta_{ss}\bar{\omega}}{\phi} = 0 \qquad \text{cooler } (S_{hl}<S\leq S_c) \tag{A-3.8c}$$

The above equations are of the form $dy/dx + py = Q,$ whose solution can be expressed as $ye^{\int pdx} = \int Qe^{\int pdx} + C.$ Hence, for each segment of the loop we obtain

$$\bar{\theta}(S) = \left[\bar{\theta}_{cl} + \frac{\bar{\omega}L_t}{nL_h}\right]e^{\frac{-nS}{\phi}} - \frac{L_t}{L_h}\frac{\bar{\omega}}{n} \qquad \text{heater } (0<S\leq S_h) \tag{A-3.9}$$

Where the boundary condition that at S=0, $\bar{\theta}(S) = \bar{\theta}_{cl}$ has been used. Similarly we get the following equation for the hot leg

$$\bar{\theta}(S) = \bar{\theta}_h e^{\frac{n}{\phi}(S_h - S)} \qquad (\text{for } S_h<S\leq S_{hl}) \tag{A-3.10}$$

Where the boundary condition that at S=S_h, $\bar{\theta}(S) = \bar{\theta}_h$ has been used. Similarly we get the following equation for the cold leg

$$\bar{\theta}(S) = \bar{\theta}_c e^{\frac{n}{\phi}(S_c - S)} \qquad (\text{for } S_c<S\leq S_t) \tag{A-3.11}$$

Where the boundary condition that at S=S_c, $\overline{\theta}(S)=\overline{\theta}_c$ has been used. For the cooler the following equation can be obtained

$$\overline{\theta}(S)=\frac{\overline{\omega}}{n}St_m(\theta_{hl})_{ss}\left[e^{\frac{St_m}{\phi}(S_{hl}-S)}-e^{\frac{n+St_m}{\phi}(S_{hl}-S)}\right]+\overline{\theta}_{hl}e^{\frac{n+St_m}{\phi}(S_{hl}-S)} \qquad \text{(for } S_{hl}<S\leq S_c\text{)} \qquad \text{(A-3.12)}$$

Where the boundary condition that at S=S_{hl}, $\overline{\theta}(S)=\overline{\theta}_{hl}$ has been used. The parameters $\overline{\theta}_{cl}$, $\overline{\theta}_h$, $\overline{\theta}_c$ and $\overline{\theta}_{hl}$ can be evaluated from the above equations by using appropriate boundary conditions. For example use of the boundary condition that at S=S_h, $\overline{\theta}(S)=\overline{\theta}_h$ in the equation for the heater gives

$$\overline{\theta}_h=\left[\overline{\theta}_{cl}+\frac{\overline{\omega}}{n}\frac{L_t}{L_h}\right]e^{\frac{-nL_h}{L_t}}-\frac{L_t}{L_h}\frac{\overline{\omega}}{n} \qquad \text{(A-3.13a)}$$

Substituting in (A-3.10) we get the following equation for the hot leg

$$\overline{\theta}(S)=\left[\overline{\theta}_{cl}+\frac{\overline{\omega}}{n}\frac{L_t}{L_h}\right]e^{\frac{-nS}{\phi}}-\frac{L_t}{L_h}\frac{\overline{\omega}}{n}e^{\frac{n}{\phi}(S_h-S)} \text{ (for } S_h<S\leq S_{hl}\text{)} \qquad \text{(A-3.13b)}$$

At S = S_{hl}, $\overline{\theta}(S)=\overline{\theta}_{hl}$. Hence

$$\overline{\theta}_{hl}=\left[\overline{\theta}_{cl}+\frac{\overline{\omega}}{n}\frac{L_t}{L_h}\right]e^{\frac{-n(L_h+L_{hl})}{L_t}}-\frac{L_t}{L_h}\frac{\overline{\omega}}{n}e^{\frac{-nL_{hl}}{L_t}} \qquad \text{(A-3.13c)}$$

Substituting this in the equation for the cooler, we get

$$\overline{\theta}(S)=\frac{\overline{\omega}}{n}St_m(\theta_{hl})_{ss}\left[e^{\frac{St_m}{\phi}(S_{hl}-S)}-e^{\frac{n+St_m}{\phi}(S_{hl}-S)}\right]+\left[\overline{\theta}_{cl}+\frac{\overline{\omega}}{n}\frac{L_t}{L_h}\right]e^{\frac{-(n+St_m)S+St_mS_{hl}}{\phi}}$$

$$-\frac{L_t}{L_h}\frac{\overline{\omega}}{n}e^{\frac{n(S_h-S)+St_m(S_{hl}-S)}{\phi}} \qquad \text{(for } S_{hl}<S\leq S_c\text{)} \qquad \text{(A-3.13d)}$$

From the above using the boundary condition that at S=S_c, $\overline{\theta}(S)=\overline{\theta}_c$ we get

$$\overline{\theta}_c=\frac{\overline{\omega}}{n}St_m(\theta_{hl})_{ss}\left(e^{\frac{-St_mL_c}{L_t}}-e^{\frac{-(n+St_m)L_c}{L_t}}\right)+\left(\overline{\theta}_{cl}+\frac{\overline{\omega}}{n}\frac{L_t}{L_h}\right)e^{-\left\{\frac{St_mL_c+n(L_h+L_{hl}+L_c)}{L_t}\right\}}$$

$$-\frac{L_t}{L_h}\frac{\overline{\omega}}{n}e^{-\left\{\frac{nL_{hl}+(n+St_m)L_c}{L_t}\right\}} \qquad \text{(A-3.13e)}$$

Using this in Eq. (A-3.11) the cold leg equation can be written as

$$\overline{\theta}(S)=\frac{\overline{\omega}}{n}St_m(\theta_{hl})_{ss}\left[e^{\frac{St_m(S_{hl}-S_c)+n(S_c-S)}{\phi}}-e^{\frac{St_m(S_{hl}-S_c)+n(S_{hl}-S)}{\phi}}\right]+\left(\overline{\theta}_{cl}+\frac{\overline{\omega}}{n}\frac{L_t}{L_h}\right)e^{\frac{St_m(S_{hl}-S_c)-nS}{\phi}}$$

$$-\frac{L_t}{L_h}\frac{\overline{\omega}}{n}e^{\frac{n(S_h-S)+St_m(S_{hl}-S_c)}{\phi}} \qquad \text{(for } S_c<S\leq S_t\text{)} \qquad \text{(A-3.13f)}$$

Using the boundary condition that at S=S_t, $\overline{\theta}(S)=\overline{\theta}_{cl}$, we can get the following expression for $\overline{\theta}_{cl}$,

$$\overline{\theta}_{cl}=\frac{\overline{\omega}}{n}\left[\frac{St_m(\theta_{hl})_{ss}e^{\frac{n(L_t-L_{cl})}{L_t}}\left(1-e^{\frac{-nL_c}{L_t}}\right)+\frac{L_t}{L_h}\left(1-e^{\frac{nL_h}{L_t}}\right)}{e^{\frac{St_mL_c+nL_t}{L_t}}-1}\right] \qquad \text{(A-3.14a)}$$

From this, $\overline{\theta}_{cl}/\overline{\omega}$ can be written as

$$\frac{\overline{\theta}_{cl}}{\overline{\omega}}=\frac{St_m(\theta_{hl})_{ss}e^{\frac{n(L_t-L_{cl})}{L_t}}\left(1-e^{\frac{-nL_c}{L_t}}\right)+\frac{L_t}{L_h}\left(1-e^{\frac{nL_h}{L_t}}\right)}{n\left(e^{\frac{St_mL_c+nL_t}{L_t}}-1\right)} \qquad \text{(A-3.14b)}$$

Expressions for $\overline{\theta}_h/\overline{\omega}$, $\overline{\theta}_{hl}/\overline{\omega}$ and $\overline{\theta}_c/\overline{\omega}$ can be obtained by using the above expression for $\overline{\theta}_{cl}/\overline{\omega}$ in equations (A-3.13a), (A-3.13c) and (A-3.13e) as follows:

$$\frac{\overline{\theta}_h}{\overline{\omega}}=\frac{St_m(\theta_{hl})_{ss}e^{\frac{nL_{hl}}{L_t}}\left(e^{\frac{nL_c}{L_t}}-1\right)+\frac{L_t}{L_h}\left(e^{\frac{-nL_h}{L_t}}-1\right)e^{\frac{(St_mL_c+nL_t)}{L_t}}}{n\left(e^{\frac{(St_mL_c+nL_t)}{L_t}}-1\right)} \qquad \text{(A-3.14c)}$$

$$\frac{\overline{\theta}_{hl}}{\overline{\omega}}=\frac{St_m(\theta_{hl})_{ss}\left(e^{n\frac{L_c}{L_t}}-1\right)+\frac{L_t}{L_h}e^{\frac{St_mL_c+n(L_t-L_{hl})}{L_t}}\left(e^{-n\frac{L_h}{L_t}}-1\right)}{n\left(e^{\frac{St_mL_c+nL_t}{L_t}}-1\right)} \qquad \text{(A-3.14d)}$$

$$\frac{\overline{\theta}_c}{\overline{\omega}} = \frac{St_m\left(\theta_{hl}\right)_{ss} e^n \left(1 - e^{\frac{-nL_c}{L_t}}\right) + \frac{L_t}{L_h} e^{\frac{nL_{cl}}{L_t}} \left(1 - e^{\frac{nL_h}{L_t}}\right)}{n\left(e^{\frac{St_m L_c + nL_t}{L_t}} - 1\right)} \tag{A-3.14e}$$

Using the expressions (A-3.9) to (A-3.12), we can find the integral $\oint \overline{\theta}(S)\, dZ$. Substituting this in Eq. (A-3.7b) we obtain the characteristic equation for stability. However, the value of the integral is different for different orientations.

HHHC Orientation

For evaluating the integral consider the figure A-2.1 with the various distances marked as shown in the direction of flow. The relations between the various lengths are given below:

$$L_t = L_h + L_{hl} + L_c + L_{cl} = L_h + L_c + 2H + L_1 + L_2 + L_3 + L_4 \tag{A-3.15}$$

$$L_{hl} = L_1 + H + L_2 \; and \; L_{cl} = L_3 + H + L_4 \tag{A-3.16}$$

The breadth of the loop, B, can be expressed as

$$B = L_1 + L_h + L_4 = L_2 + L_c + L_3 \tag{A-3.17}$$

For generality, the lengths L_1, L_2, L_3 and L_4 are considered to be unequal. The cumulative lengths, s_1, s_2, s_3 and s_4 can be expressed as

$$s_1 = L_h + L_1 \; ; \; s_2 = s_1 + H \; ; \; s_3 = s_2 + B = s_c + L_3 = L_h + L_{hl} + L_c + L_3 \; \& \; s_4 = s_3 + H \tag{A-3.18}$$

The nondimensional lengths S_2 and S_4 can be expressed as

$$S_2 = S_1 + 1 \; and \; S_4 = S_3 + 1 \tag{A-3.19}$$

The integral $\oint \overline{\theta}(S)\, dZ$ can be expressed as

$$\oint \overline{\theta}(S)\, dZ = \int_{S_1}^{S_2} \left\{ \overline{\theta}(S) \right\}_{hot\ leg} dZ + \int_{S_3}^{S_4} \left\{ \overline{\theta}(S) \right\}_{cold\ leg} dZ \tag{A-3.20}$$

For the hot leg dZ=dS and for the cold leg dZ= -dS. Hence, using (A-3.10) and (A-3.11) we can obtain

$$\oint \overline{\theta}(S)\, dZ = \int_{S_1}^{S_1+1} \overline{\theta}_h e^{\frac{n(S_h - S)}{\phi}} dS - \int_{S_3}^{S_3+1} \overline{\theta}_c e^{\frac{n(S_c - S)}{\phi}} dS \tag{A-3.21}$$

Integrating and substituting the limits yield

$$\oint \overline{\theta}(S)\, dZ = \frac{\phi}{n}\left(1 - e^{\frac{-n}{\phi}}\right)\left\{ \overline{\theta}_h e^{\frac{-nL_1}{L_t}} - \overline{\theta}_c e^{\frac{-nL_3}{L_t}} \right\} \tag{A-3.22}$$

$$\frac{\bar{I}}{\bar{\omega}} = \frac{1}{\bar{\omega}}\oint\bar{\theta}(S)\,dZ = \frac{\phi}{n}\left(1-e^{\frac{-n}{\phi}}\right)\left\{\frac{\bar{\theta}_h}{\bar{\omega}}e^{\frac{-nL_1}{L_t}} - \frac{\bar{\theta}_c}{\bar{\omega}}e^{\frac{-nL_3}{L_t}}\right\} \tag{A-3.23}$$

$\bar{\theta}_h/\bar{\omega}$ and $\bar{\theta}_c/\bar{\omega}$ are obtained from Eq. (A-3.14c) and (A-3.14e) respectively. If $L_1 = L_2 = L_x$, then this reduces to

$$\frac{\bar{I}}{\bar{\omega}} = \frac{1}{\bar{\omega}}\oint\bar{\theta}(S)\,dZ = \frac{\phi}{n}\left(1-e^{\frac{-n}{\phi}}\right)\left(e^{\frac{-nL_x}{L_t}}\right)\left\{\frac{\bar{\theta}_h-\bar{\theta}_c}{\bar{\omega}}\right\} \tag{A-3.24}$$

Using Eqs. (A-3.14c) and (A-3.14e), the following expression for $\left(\bar{\theta}_h-\bar{\theta}_c\right)/\bar{\omega}$ can be obtained as

$$\frac{\bar{\theta}_h-\bar{\theta}_c}{\bar{\omega}} = \frac{St_m(\theta_{hl})_{ss}\left\{e^{\frac{nL_{hl}}{L_t}}\left(e^{\frac{nL_c}{L_t}}-1\right)-e^{n}\left(1-e^{\frac{-nL_c}{L_t}}\right)\right\}+\frac{L_t}{L_h}\left\{e^{\frac{St_mL_c+nL_t}{L_t}}\left(e^{\frac{-nL_h}{L_t}}-1\right)-e^{\frac{nL_{cl}}{L_t}}\left(1-e^{\frac{nL_h}{L_t}}\right)\right\}}{n\left(e^{\frac{St_mL_c+nL_t}{L_t}}-1\right)}$$

HHVC Orientation

Refer to Fig. A-2.2 for the geometry and co-ordinate system considered. For S_1 to S_2 dZ = dS, and for S_3 to S_4, dZ= - dS. Hence

$$\begin{aligned}\oint\bar{\theta}(S)\,dZ = &\int_{S_1}^{S_1+1}\bar{\theta}_h e^{\frac{n(S_h-S)}{\phi}}\,dS - \int_{S_3}^{S_{hl}}\bar{\theta}_h e^{\frac{n(S_h-S)}{\phi}}\,dS - \int_{S_{hl}}^{S_c}\bar{\theta}_{hl}e^{\frac{n+St_m(S_{hl}-S)}{\phi}}\,dS - \\ &\frac{\bar{\omega}}{n}St_m(\theta_{hl})_{ss}\int_{S_{hl}}^{S_c}\left(e^{\frac{St_m(S_{hl}-S)}{\phi}}-e^{\frac{n+St_m(S_{hl}-S)}{\phi}}\right)dS - \int_{S_c}^{S_4}\bar{\theta}_c e^{\frac{n(S_c-S)}{\phi}}\,dS\end{aligned} \tag{A-3.25}$$

On integration and substitution of limits yield the following equation for $\bar{I}/\bar{\omega}$.

$$\begin{aligned}\frac{\bar{I}}{\bar{\omega}} = &\frac{\bar{\theta}_h}{\bar{\omega}}\frac{\phi}{n}\left\{e^{\frac{-nL_1}{L_t}}\left(1-e^{\frac{-n}{\phi}}\right)+e^{\frac{-nL_{hl}}{L_t}}\left(1-e^{\frac{nL_2}{L_t}}\right)\right\}+\frac{\phi}{n}(\theta_{hl})_{ss}\left\{e^{\frac{-St_mL_c}{L_t}}-1+\frac{St_m}{n+St_m}\left(1-e^{-\left(\frac{n+St_m}{L_t}\right)L_c}\right)\right\} \\ &+\frac{\bar{\theta}_{hl}}{\bar{\omega}}\left(\frac{\phi}{n+St_m}\right)\left[e^{\frac{-(n+St_m)L_c}{L_t}}-1\right]+\frac{\bar{\theta}_c}{\bar{\omega}}\frac{\phi}{n}\left[e^{\frac{-nL_3}{L_t}}-1\right]\end{aligned} \tag{A-3.26}$$

The parameters $\bar{\theta}_h/\bar{\omega}, \bar{\theta}_{hl}/\bar{\omega},$ and $\bar{\theta}_c/\bar{\omega}$ are evaluated using equations (A-3.14c), (A-3.14d) and (A-3.14e) respectively.

VHHC Orientation

Refer to Fig. A-2.3 for the geometry and co-ordinate system considered. For S_1 to S_2 dZ = dS, and for S_3 to S_4, dZ= - dS. Hence,

$$\int \bar{\theta}(S)\,dZ = \int_0^{S_h}\left[\left(\bar{\theta}_{cl} + \frac{\bar{\omega}}{n}\frac{L_t}{L_h}\right)e^{\frac{-nS}{\phi}} - \frac{\bar{\omega}}{n}\frac{L_t}{L_h}\right]dS + \int_{S_h}^{S_2}\bar{\theta}_h e^{\frac{n(S_h-S)}{\phi}}\,dS - \int_{S_3}^{S_{3+1}}\bar{\theta}_c e^{\frac{n(S_c-S)}{\phi}}\,dS$$

$$+ \int_{S_1}^{S_t}\bar{\theta}_c e^{\frac{n(S_c-S)}{\phi}}\,dS \qquad \text{(A-3.27)}$$

$$\frac{\bar{I}}{\bar{\omega}} = \frac{\bar{\theta}_{cl}}{\bar{\omega}}\frac{\phi}{n}\left(1-e^{\frac{-nL_h}{L_t}}\right) + \frac{L_t}{nL_h}\left\{\frac{\phi}{n}\left(1-e^{\frac{-nL_h}{L_t}}\right) - \frac{L_h}{H}\right\} + \frac{\bar{\theta}_h}{\bar{\omega}}\frac{\phi}{n}\left[1-e^{\frac{-nL_1}{L_t}}\right] + \frac{\bar{\theta}_c}{\bar{\omega}}\frac{\phi}{n}\left[\frac{e^{\frac{-nH}{L_t}}-1}{e^{\frac{nL_3}{L_t}}} + \frac{e^{\frac{nL_4}{L_t}}-1}{e^{\frac{nL_{cl}}{L_t}}}\right] \qquad \text{(A-3.28)}$$

The parameters $\bar{\theta}_{cl}/\bar{\omega}$, $\bar{\theta}_h/\bar{\omega}$ and $\bar{\theta}_c/\bar{\omega}$ are evaluated using equations (A-3.14b), (A-3.14c) and (A-3.14e) respectively.

VHVC Orientation

Refer to Fig. A-2.4 for the geometry and co-ordinate system considered. For S_1 to S_2 dZ = dS, and for S_3 to S_4, dZ= - dS. Hence,

$$\bar{I} = \int_0^{S_h}\left\{\left(\bar{\theta}_{cl} + \frac{\bar{\omega}}{n}\frac{L_t}{L_h}\right)e^{\frac{-nS}{\phi}} - \frac{\bar{\omega}}{n}\frac{L_t}{L_h}\right\}dS + \int_{S_h}^{S_2}\bar{\theta}_h e^{\frac{n}{\phi}(S_h-S)}\,dS - \int_{S_3}^{S_{hl}}\bar{\theta}_h e^{\frac{n}{\phi}(S_h-S)}\,dS$$

$$- \int_{S_{hl}}^{S_c}\left\{\frac{\bar{\omega}}{n}St_m(\theta_{hl})_{ss}\left(e^{\frac{St_m(S_{hl}-S)}{\phi}} - e^{\frac{n+St_m}{\phi}(S_{hl}-S)}\right) + \bar{\theta}_{hl}e^{\frac{(n+St_m)}{\phi}(S_{hl}-S)}\right\}dS - \int_{S_c}^{S_4}\bar{\theta}_c e^{\frac{n}{\phi}(S_c-S)}\,dS$$

$$- \int_{S_1}^{S_t}\bar{\theta}_c e^{\frac{n}{\phi}(S_c-S)}\,dS \qquad \text{(A-3.29)}$$

After integration and substitution of limits we obtain

$$\frac{\bar{I}}{\bar{\omega}} = \frac{\bar{\theta}_{cl}}{\bar{\omega}}\frac{\phi}{n}\left(1-e^{\frac{-nL_h}{L_t}}\right) + \frac{L_t^2}{n^2L_hH}\left(1-e^{\frac{-nL_h}{L_t}} - \frac{nL_h}{L_t}\right) + \frac{\bar{\theta}_h}{\bar{\omega}}\frac{\phi}{n}\left[1-e^{\frac{-nL_1}{L_t}} + e^{\frac{-nL_{hl}}{L_t}}\left(1-e^{\frac{-nL_2}{L_t}}\right)\right] +$$

$$\frac{\phi(\theta_{hl})_{ss}}{n(n+St_m)}\left[n\left(e^{\frac{-St_mL_c}{L_t}}-1\right) + St_m e^{\frac{-St_mL_c}{L_t}}\left(1-e^{\frac{-nL_c}{L_t}}\right)\right] + \frac{\bar{\theta}_{hl}}{\bar{\omega}}\frac{\phi}{n+St_m}\left[e^{\frac{-(n+St_m)L_c}{L_t}}-1\right] +$$

$$\frac{\bar{\theta}_c}{\bar{\omega}}\frac{\phi}{n}\left\{e^{\frac{-nL_3}{L_t}} - 1 + e^{\frac{-nL_{cl}}{L_t}}\left(e^{\frac{nL_4}{L_t}}-1\right)\right\} \qquad \text{(A-3.30)}$$

The parameters $\bar{\theta}_{cl}/\bar{\omega}$, $\bar{\theta}_h/\bar{\omega}$, $\bar{\theta}_{hl}/\bar{\omega}$ and $\bar{\theta}_c/\bar{\omega}$ are evaluated using equations (A-3.14b), (A-3.14c), (A-3.14d) and (A-3.14e) respectively.

HHVC Orientation with anticlockwise flow

Refer to Fig. A-2.5 for the geometry and co-ordinate system considered. For S_1 to S_2 dZ = dS, and for S_3 to S_4, dZ= - dS. Hence,

$$\oint\bar{\theta}(S)dZ = \int_{S_1}^{S_{hl}}\bar{\theta}_h e^{\frac{n}{\phi}(S_h-S)}dS + \int_{S_{hl}}^{S_c}\left\{\frac{\bar{\omega}}{n}St_m(\theta_{hl})_{ss}\left(e^{\frac{St_m(S_{hl}-S)}{\phi}} - e^{\frac{n+St_m}{\phi}(S_{hl}-S)}\right) + \bar{\theta}_{hl}e^{\frac{(n+St_m)}{\phi}(S_{hl}-S)}\right\}dS$$

$$+ \int_{S_c}^{S_2}\bar{\theta}_c e^{\frac{n}{\phi}(S_c-S)}dS - \int_{S_3}^{S_{3+1}}\bar{\theta}_c e^{\frac{n}{\phi}(S_c-S)}dS \qquad \text{(A-3.31)}$$

After integration and substitution of the limits and simplifying we obtain

$$\frac{\bar{I}}{\bar{\omega}} = \frac{\bar{\theta}_h}{\bar{\omega}}\frac{\phi}{n}e^{\frac{-nL_1}{L_t}}\left(1-e^{\frac{-nL_2}{L_t}}\right) + \frac{\phi}{n}\frac{(\theta_{hl})_{ss}}{n+St_m}\left\{n\left(1-e^{\frac{-St_mL_c}{L_t}}\right) - St_m e^{\frac{-St_mL_c}{L_t}}\left(1-e^{\frac{-nL_c}{L_t}}\right)\right\}$$

$$+\frac{\bar{\theta}_c}{\bar{\omega}}\frac{\phi}{n}\left\{1-e^{\frac{-nL_3}{L_t}} - \left(1-e^{\frac{-n}{\phi}}\right)e^{\frac{-n}{L_t}(L_3+L_1+L_h+L_4)}\right\} + \frac{\bar{\theta}_{hl}}{\bar{\omega}}\frac{\phi}{n+St_m}\left(1-e^{\frac{-(n+St_m)L_c}{L_t}}\right) \qquad \text{(A-3.32)}$$

The parameters $\bar{\theta}_h/\bar{\omega}$, $\bar{\theta}_{hl}/\bar{\omega}$ and $\bar{\theta}_c/\bar{\omega}$ are evaluated using equations (A-3.14c), (A-3.14d) and (A-3.14e) respectively.

APPENDIX-4: Linear Stability analysis of two-phase NCS

The analysis is carried out for a simple loop as shown in Fig. A-4.1 where complete separation of the steam-water mixture is assumed to take place in the steam drum. The separated water is assumed to completely mix with the feed water in the steam drum. For the sake of simplicity we use further simplifying assumptions like uniform axial heat flux in the heated section and insulated piping. In addition, the effect of $\partial p / \partial t$ is also neglected. With these assumptions, the governing equations can be rewritten as

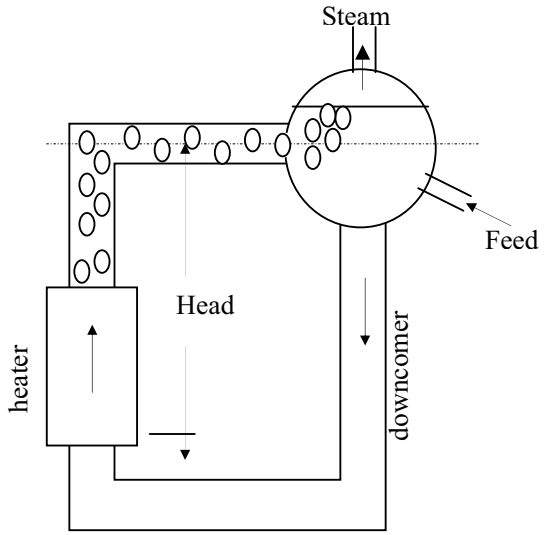

FIG. A-4.1. A simple two-phase NC loop

$$A\frac{\partial \rho}{\partial t}+\frac{\partial w}{\partial z}=0 \tag{A-4.1}$$

$$\frac{1}{A}\frac{\partial w}{\partial t}+\frac{1}{A^2}\frac{\partial}{\partial z}(w^2/\rho)+\rho g\cos\phi+\frac{f}{2DA^2}(w^2/\rho)+\frac{\partial p}{\partial z}=0 \tag{A-4.2}$$

The pressure drop due to bends, restrictions, spacers, etc. was estimated as

$$\Delta p_k = KW^2/2\rho A^2 \tag{A-4.2a}$$

$$\rho A\frac{\partial h}{\partial t}+w\frac{\partial h}{\partial z}=\begin{cases} q_h''' A & \text{heated region,} \\ 0 & \text{adiabatic region.}\end{cases} \tag{A-4.3}$$

In addition an equation of state is required for the density and is given by

$$\rho = f(p,h) \tag{A-4.4}$$

The steady state solution, which is essential for performing the linear stability analysis, can be obtained by dropping the time derivatives from the above equations. These are

$$\frac{\partial w}{\partial z}=0 \tag{A-4.5}$$

$$\frac{1}{A^2}\frac{\partial}{\partial z}(w^2/\rho)+\rho g\cos\phi+\frac{f}{2DA^2}(w^2/\rho)+\frac{\partial p}{\partial z}=0 \tag{A-4.6}$$

$$w\frac{\partial h}{\partial z}=\begin{cases}q_h'''A & heated\ region,\\ 0 & adiabatic\ region.\end{cases} \tag{A-4.7}$$

Equations (5) to (7) are solved together to obtain the steady state flow rate for a given power and reactor inlet temperature or specific enthalpy conditions as follows.

(i) Assume an initial flow rate

(ii) With this flow rate, obtain the enthalpy in the heated region at any axial distance (z) as

$$h(z)=h_{in}+\frac{q_h'''Az}{w} \tag{A-4.8}$$

The specific enthalpy is constant in the adiabatic regions so that h(z)=h_{in} for the downcomer to the heater inlet and h(z) = h_o from heater outlet to the SD. The heater outlet enthalpy h_o can be calculated from Eq. (A-4.8) as

$$h_o=h_{in}+\frac{q_h'''AL_h}{w} \tag{A-4.9}$$

where L_h is the total length of the heated region. At steady state, the feed water flow rate is equal to the steam flow rate. Assuming complete mixing in the SD, the enthalpy h_{in} can be calculated as

$$h_{in}=(1-x_e)h_f+x_e h_{FD} \tag{A-4.10}$$

where x_e is the exit quality and h_{FD} is the feed water enthalpy. Noting that $h_o= x_e h_g+ (1-x_e)h_f$, the exit quality can be calculated from Eq. (A-4.9) as

$$x_e=\frac{h_{in}-h_f}{h_{fg}}+\frac{Q_h AL_h}{wh_{fg}} \tag{A-4.11}$$

(iii) From the specific enthalpy, the length of the single-phase region, is determined as

$$L_{sp}=\frac{w(h_f-h_{in})}{q_h'''A} \tag{A-4.12}$$

In the single-phase heated region, the variation of density is obtained using the Boussinesq approximation as given by

$$\rho(z)=\rho_o[1-\sigma(T(z)-T_{in})]\cong\rho_o\left(1-\frac{\sigma(h(z)-h_{in})}{Cp}\right) \tag{A-4.13}$$

where σ is the volumetric thermal expansion coefficient and Cp is the specific heat of the mixture. In the two-phase heated region, the variation of density is given by

$$\rho(z) = \alpha(z)\rho_g + (1-\alpha(z))\rho_f \qquad \text{(A-4.14)}$$

where $\alpha(z)$ is the void fraction at any axial location, which is calculated considering homogeneous two-phase mixture. The steady state mass flow rate is calculated by numerically integrating Eq. (A-4.6) along the loop. The integral momentum equation for the steady state case can be obtained as

$$\frac{\oint d(w^2 v)}{A^2} + g\oint \rho dz + \frac{w^2}{2A^2\rho_f}\left[\frac{f_f L_{sp}\rho_f}{D\rho_{in}} + K_i\frac{\rho_f}{\rho_{in}} + \left(\bar{\phi}^2_{LO}L_{tp}\right)_h + \left(\phi^2_{LO}L_{tp}\right)_p + K_o\frac{\rho_f}{\rho_{tp}}\right] = 0 \qquad \text{(A-4.15)}$$

While the density at any axial distance is known from equations (A-4.13) and (A-4.14), the friction factor in the single-phase region, is obtained from the local Reynolds number as follows.

$$f_{1\phi} = 64/\mathrm{Re} \qquad \text{for laminar flow} \qquad \text{(A-4.16a)}$$

$$f_{1\phi} = 0.316/\mathrm{Re}^{0.25} \qquad \text{for turbulent flow} \qquad \text{(A-4.16b)}$$

In the two-phase region, a two-phase friction factor multiplier (Φ^2_{lo}) was used to estimate the frictional pressure loss as given below.

$$\Phi^2_{lo} = \frac{(dp/dz)_{2\phi}}{(dp/dz)_{1\phi}} \qquad \text{(A-4.17)}$$

In this work, the Baroczy (1966) model was used to evaluate the two-phase multiplier.
(vi) After calculating all the terms in the Eq. (A-4.15), check whether the equation is satisfied with the assumed flow rate. If not, then steps i) to vi) are iterated until Eq. (A-4.15) is satisfied within a chosen convergence criterion.

Flow distribution in the parallel channels

The gross flow obtained from Eq. (A-4.15) is divided into the channels of the reactor connected between the inlet header and the steam drum. The flow distribution in the channels is not uniform because of unequal heat generation in the channels. For obtaining the channel flow distribution, the pressure variation in the header and the steam drum is neglected. Since all parallel channels are connected between the inlet header and the steam drum, we have

$$\Delta p_{H-SD} = (\Delta p_{ch})_1 = (\Delta p_{ch})_2 = (\Delta p_{ch})_i \qquad \text{(A-4.18)}$$

To obtain $(\Delta p_{ch})_i$ Eq. (A-4.6) is integrated from the header to the SD. Similarly, the pressure drop between the steam drum and the inlet header is estimated as

$$\Delta p_{SD-H} = -\rho_{in} g\Delta Z + \frac{w_t^2}{2\rho_{in}A^2}\left(\frac{fL}{D} + K\right) \qquad \text{(A-4.19)}$$

where ΔZ is the elevation difference between the steam drum water level and the inlet header and w_t is the total loop flow rate and can be expressed as

$$w_t = \sum_{i=1}^{N} (w_{ch})_i \tag{A-4.20}$$

The total flow rate w_t and individual channel flow rates $(w_{ch})_i$ are estimated by solving equations (A-4.18) to (A-4.20) iteratively with the condition that $\Delta p_{H-SD} + \Delta p_{SD-H} = 0$.

Linear Stability Analysis

The conservation equations (A-4.1) to (A-4.3) are perturbed by introducing small perturbations over the steady state as follows

$$w = w_{ss} + w';\ h = h_{ss} + h';\ p = p_{ss} + p';\ v = v_{ss} + v';\ q'''_h = q'''_{h,ss} + \left(q'''_h\right)' \tag{A-4.21a}$$

where $w' = \bar{w}(z)\varepsilon e^{st};\ h' = \bar{h}(z)\varepsilon e^{st};\ p' = \bar{p}(z)\varepsilon e^{st};\ v' = \bar{v}(z)\varepsilon e^{st};\ \left(q'''_h\right) = \bar{q}'''_h(z)\varepsilon e^{st}$ (A-4.21b)

In Eq. (A-4.21) ε is a small quantity and $\bar{w}, \bar{h}, \bar{p}, \bar{v}$ *and* $\bar{q}'''_h$ are the amplitudes of the perturbed flow rate, enthalpy, pressure, specific volume and heat added per unit volume of coolant respectively and s is the stability parameter. With these substitutions, the perturbed conservation equations after linearization can be written as follows for the single-phase region.

$$\frac{dw'}{dz} = 0 \tag{A-4.22}$$

$$\frac{dh'}{dz} + \frac{\rho_{in} A s h'}{w_{ss}} = \begin{cases} -\dfrac{w' q'''_{h,ss} A}{w_{ss}^2} + \dfrac{\left(q'''_h\right)' A}{w_{ss}} & \textit{heated region} \\ 0 & \textit{adiabatic region} \end{cases} \tag{A-4.23}$$

$$\frac{dp'}{dz} + w'\left(\frac{s}{A} + \frac{f w_{ss}}{\rho_{in} D A^2}\right) - \frac{g\beta\rho_{in}}{Cp} = 0 \tag{A-4.24}$$

Similarly, the perturbed conservation equations for the two-phase region are

$$\frac{dw'}{dz} = \frac{As}{v_{ss}^2}\frac{v_{fg}}{h_{fg}} h' \tag{A-4.25}$$

$$\frac{dh'}{dz} + \frac{sA}{v_{ss} w_{ss}} h' = \begin{cases} -\dfrac{q'''_{h,ss} A w'}{w_{ss}^2} + \dfrac{\left(q'''_h\right)' A}{w_{ss}} & \textit{heated region} \\ 0 & \textit{adiabatic region} \end{cases} \tag{A-4.26}$$

$$\frac{dp'}{dz} + w'\left(\frac{s}{A} + \frac{f w_{ss} v_{ss}}{D A^2}\right) + h'\frac{v_{fg}}{h_{fg}}\frac{f w_{ss}^2}{2DA^2} - \frac{g}{v_{ss}^2} + \frac{2s w_{ss}}{A v_{ss}} + \frac{w_{ss}^2}{A^2}\frac{v_{fg}}{h_{fg}}\frac{dh'}{dz} = 0 \tag{A-4.27}$$

Solutions of the perturbed differential equations for the heated single-phase region can be obtained as

$$w' = w'_{in} = \text{constant} \tag{A-4.28}$$

$$h' = \frac{1-e^{-\tau_{sp}s}}{\rho_{ss,av}s}\left(\frac{-q'''_{h,ss}w'}{w_{ss}} + \left(q'''_h\right)'\right) \tag{A-4.29}$$

where h'_{in} is the perturbed enthalpy at the inlet of core and $\tau_{sp} = (\rho_{ss,av}AL_{sp} / w_{ss})$ is the residence time of the fluid in the single-phase region of the heater.

$$-\Delta p'_{sp} = \left(\frac{s}{A} + \frac{fw_{ss}}{\rho_{ss,av}DA^2}\right)w'L_{sp} - \frac{g\sigma}{Cps}\left(\left(q'''_h\right)' - \frac{q'''_{h,ss}w'}{w_{ss}}\right)\left(L_{sp} + \frac{w_{ss}\left(e^{-\tau_{sp}s}-1\right)}{\rho_{ss,av}As}\right) \tag{A-4.30}$$

In the adiabatic single-phase region, the perturbed equations for flow rate, enthalpy and pressure drop were obtained from Eqs. (A-4.28) to (A-4.30) respectively, by setting Q_{ss} and Q' equal to zero. For the two-phase heated region

$$w' = w'_{sp} + \left(\frac{sA}{v_{ss}^2}\frac{v_{fg}}{h_{fg}}\right)\left[\frac{X}{r_1}\left(e^{r_1L_c} - e^{r_1L_{sp}}\right) + \frac{Y}{r_2}\left(e^{r_2L_c} - e^{r_2L_{sp}}\right)\right] \tag{A-4.31}$$

$$h' = Xe^{r_1L_c} + Ye^{r_2L_c} \tag{A-4.32}$$

$$\begin{aligned}
-\Delta p' = {} & \left(\frac{s}{A} + \frac{fw_{ss}v_{ss,av}}{DA^2}\right) \\
& \left[w'_{sp}L_{tp} + \frac{Asv_{fg}}{v_{ss,av}^2h_{fg}}\left\{\frac{X}{r_1}\left\{\frac{1}{r_1}\left(e^{r_1L_c} - e^{r_1L_{sp}}\right) - e^{r_1L_{sp}}L_{tp}\right\} + \frac{Y}{r_2}\left\{\frac{1}{r_2}\left(e^{r_2L_c} - e^{r_2L_{sp}}\right) - e^{r_2L_{sp}}L_{tp}\right\}\right\}\right] \\
& \frac{v_{fg}}{h_{fg}}\left[\frac{fw_{ss}^2}{2DA^2} - \frac{g}{v_{ss,av}^2} + \frac{2w_{ss}s}{Av_{ss,av}}\right]\left[\frac{X}{r_1}\left(e^{r_1L_c} - e^{r_1L_{sp}}\right) + \frac{Y}{r_2}\left(e^{r_2L_c} - e^{r_2L_{sp}}\right)\right] + \\
& \frac{w_{ss}^2}{A^2h_{fg}}\left[X\left(e^{r_1L_c} - e^{r_1L_{sp}}\right) + Y\left(e^{r_2L_c} - e^{r_2L_{sp}}\right)\right]
\end{aligned} \tag{A-4.33}$$

where $X = \left[-h'_{sp}\left(r_2 + As\rho_f / w_{ss}\right) - q'''_{h,ss}Aw'_{sp} / w_{ss}^2 + \left(q'''_h\right)'A / w_{ss}\right] / \left(r_1 - r_2\right)e^{r_1L_{sp}}$ (A-4.34)

$$Y = \left(h'_{sp} - Xe^{r_1L_{sp}}\right) / e^{r_2L_{sp}} \tag{A-4.35}$$

$$r_{1,2} = \frac{1}{2}\left[-\frac{As}{v_{ss,av}w_{ss}} \pm \left(\left\{\frac{As}{v_{ss,av}w_{ss}}\right\}^2 - \frac{4q'''_{h,ss}}{v_{ss,av}^2}\frac{A^2s}{w_{ss}^2}\frac{v_{fg}}{h_{fg}}\right)^{1/2}\right] \tag{A-4.36}$$

where the positive sign applies for r_1 and negative sign applies for r_2. h'_{sp} is the perturbed enthalpy at the inlet of boiling region of the channel. In the adiabatic two-phase region,

$$w' = w'_{in} + (w_{ss}/v_{ss})(v_{fg}/h_{fg})h'_{in}\left[1-e^{-\tau_L s}\right] \tag{A-4.37}$$

$$h' = h'_{in}e^{-\tau_L s} \tag{A-4.38}$$

$$\begin{aligned}-\Delta p' = &\left[\frac{s}{A}+\frac{fw_{ss}v_{ss}}{DA^2}\right]\left[w'_{in}L+\frac{w_{ss}v_{fg}}{v_{ss}h_{fg}}h'_m\left\{L+\frac{w_{ss}v_{ss}}{As}\left(e^{-\tau_L s}-1\right)\right\}\right]\\ &-\frac{v_{fg}}{h_{fg}}\left[\frac{fw_{ss}^2}{2DA^2}-\frac{g}{v_{ss}^2}+\frac{2w_{ss}s}{Av_{ss}}\right]\left[\left\{e^{-\tau_L s}-1\right\}h'_{in}\frac{w_{ss}v_{ss}}{As}\right]+\frac{w_{ss}^2}{A^2}\frac{v_{fg}}{h_{fg}}\left(e^{-\tau_L s}-1\right)h'_{in}\end{aligned} \tag{A-4.39}$$

where $\tau_L = (\rho_{in}AL/w_{ss})$ (A-4.40)

Similarly, the perturbed pressure drop due to bends, orifices and other restrictions in the single-phase region is given by

$$\Delta p'_{k,sp} = (K_{sp}/\rho A^2)w_{ss}w'_{in} \tag{A-4.41}$$

In the two-phase region,

$$\Delta p'_{k,tp} = (K_{tp}/2A^2)\left[w_{ss}^2 h'_{in}(v_{fg}/h_{fg}) + 2w_{ss}v_{ss}w'_{in}\right] \tag{A-4.42}$$

The perturbed heat added/unit volume of coolant, $\left(Q'_h\right)$, that appears in the above equations depends on the neutron kinetics and dynamics of heat transfer. This can be evaluated from the point kinetics model as follows:

$$\frac{dn}{dt} = \frac{k(1-\beta)-1}{l}n + \sum_{m=1}^{6}\lambda_m C_m \tag{A-4.43}$$

$$\frac{dC_m}{dt} = \frac{k\beta n}{l} - \lambda_m C_m \tag{A-4.44}$$

where n is the neutron density, k is the effective multiplication factor, β is the delayed neutron fraction, λ_m and C_m are the decay constant and precursor concentration of delayed neutrons of group m respectively. Eqs. (A-4.43) and (A-4.44) are linearized by perturbing over the steady state as before to obtain

$$\frac{n'}{n_{ss}} = \frac{k'}{ls + \sum_{m=1}^{6}\frac{s\beta_m}{s+\lambda_m}} \tag{A-4.45}$$

where n' is the perturbed neutron density and k' is the perturbed reactivity which is related to the void reactivity coefficient and Doppler coefficient as

$$k' = C_\alpha \gamma'_{av} + C_D T'_{f,av} \tag{A-4.46}$$

In the above equation, γ'_{av} and $T'_{f,av}$ are the perturbed void fraction and fuel temperature respectively averaged over the heated channel length. They can be estimated from the coolant density and the fuel heat transfer equations as discussed below.

Fuel heat transfer model

Assuming only radial heat transfer, the fuel heat transfer equation can be written as

$$m_f C_f \frac{dT_{f,av}}{dt} = Q_h(t) - H_f a_f (T_{f,av}(t) - T_{sat}) \tag{A-4.47}$$

where m_f is the mass of fuel rods, C_f is the specific heat capacity of fuel, H_f is an effective heat transfer coefficient, $Q_h(t)$ is the heat generation rate in the fuel rods, $T_{f,av}(t)$ is the length average fuel temperature, a_f is the heat transfer area of fuel rods and T_{sat} is the coolant saturation temperature. Perturbing Eq. (A-4.47) over the steady state for $T_{f,av}(t)$ and $Q(t)$ and canceling the steady state terms, we get

$$T'_{f,av}(m_f C_f s + H_f a_f) = Q'_h, \tag{A-4.48}$$

where Q'_h is the perturbed heat generation rate in the fuel rod. Applying the heat balance equation for the heat transfer from fuel to coolant

$$H_f a_f (T_{f,av} - T_{sat}) = q'''_h A_c L_c . \tag{A-4.49}$$

Perturbing Eq. (A-4.49) over the steady state and canceling the steady state terms we get

$$T'_{f,av} = \left(q'''_h\right)' A_c L_c / H_f a_f . \tag{A-4.50}$$

Substituting Eq. (A-4.50) into Eq. (A-4.48) and rearranging we get

$$\left(q'''_h\right)' = q'''_{h,ss} \frac{Q'_h}{Q_{h,ss}} \left[\frac{1}{1 + m_f C_f s / H_f a_f} \right] \tag{A-4.51}$$

Since the heat generation rate in fuel is proportional to the neutron density, Eqs. (A-4.45) and (A-4.46) can be substituted into Eq. (A-4.51) to yield

$$\left(q'''_h\right)' = G_f \gamma'_{av}, \tag{A-4.52}$$

$$\text{where } G_f = \frac{C_\alpha / (1+\tau_f s)(ls + \sum_{m=1}^{6} \frac{s\beta_m}{s+\lambda_m})}{\frac{1}{q'''_{h,ss}} - \frac{C_D A_c L_c}{H_f a_f (1+\tau_f s)(ls + \sum_{m=1}^{6} \frac{s\beta_m}{s+\lambda_m})}}, \tag{A-4.53}$$

and $\tau_f = \frac{m_f C_f}{H_f a_f}$ is the fuel thermal time constant. The density of two-phase mixture is given by

$$\rho = \gamma\rho_g + (1-\gamma)\rho_f \,. \tag{A-4.54}$$

Perturbing Eq. (A-4.52) over the steady state and canceling for steady state condition, we get

$$\gamma^{'} = -\rho^{'} / \rho_{fg} = (\rho_{ss}^2 / \rho_{fg}) \frac{v_{fg}}{h_{fg}} h^{'}. \tag{A-4.55}$$

The channel average perturbed void fraction can be obtained by integration as

$$\gamma_{av}^{'} = \frac{1}{L_c} \int_{z=L_{sp}}^{L_c} \frac{\rho_{ss}^2 v_{fg}}{\rho_{fg} h_{fg}} h^{'} dz \,, \tag{A-4.56}$$

which can be approximated after some algebraic simplification as

$$\gamma_{av}^{'} = \psi_1 w_{in}^{'} + \psi_2 q_h^{'} \,, \tag{A-4.57}$$

$$\text{where} \quad \psi_1 = \frac{1}{L_c} \frac{v_{fg}}{h_{fg}} \frac{1}{v_{ss,av}^2} \frac{1}{h_{fg}} \left[\frac{X_1}{r_1} (e^{r_1 L_c} - e^{r_1 L_{sp}}) + \frac{X_2}{r_2} \left(e^{r_2 L_c} - e^{r_2 L_{sp}} \right) \right], \tag{A-4.58}$$

$$\psi_2 = \frac{1}{L_c} \frac{v_{fg}}{h_{fg}} \frac{1}{v_{ss,av}^2} \frac{1}{h_{fg}} \left[\frac{Y_1}{r_1} (e^{r_1 L_c} - e^{r_1 L_{sp}}) + \frac{Y_2}{r_2} \left(e^{r_2 L_c} - e^{r_2 L_{sp}} \right) \right], \tag{A-4.59}$$

$$X_1 = \frac{-q_{h,ss}^{'''} A}{w_{ss}^2} \left[1 + \left[\left(e^{-\tau_{sp} s} - 1 \right) / \rho_{in} s \right] (w_{ss} / A)(r_2 + \frac{As\rho_{in}}{w_{ss}}) \right] / \left[(r_1 - r_2) e^{r_1 L_{sp}} \right], \tag{A-4.60}$$

$$X_2 = \left[\{ \ (q_{h,ss}^{'''} / w_{ss})(e^{-\tau_{sp} s} - 1) / \rho_{in} s \ \} - X_1 e^{r_1 L_{sp}} \right] / e^{r_2 L_{sp}} \,, \tag{A-4.61}$$

$$Y_1 = \left[\left(\frac{e^{-\tau_{sp} s} - 1}{\rho_{in} s} \right) \left(r_2 + \frac{As\rho_{in}}{w_{ss}} \right) + \frac{A}{w_{ss}} \right] / (r_1 - r_2) e^{r_1 L_{sp}} \,, \tag{A-4.62}$$

$$Y_2 = -\left[\frac{e^{-\tau_{sp} s} - 1}{\rho_{in} s} + Y_1 e^{r_1 L_{sp}} \right] / e^{r_2 L_{sp}} \,. \tag{A-4.63}$$

Substituting Eq. (A-4.57) into Eq. (A-4.52) an expression for the perturbed heat added/unit volume of coolant $\left(q_h^{'''}\right)$ to any channel i for a perturbation of channel inlet flow rate ($w_{in}^{'}$) in the i_{th} channel can be easily obtained as given by

$$(q_h^{'''})_i^{'} = (\frac{G_f \psi_1}{1 - G_f \psi_2})_i (w_{in}^{'})_i \,. \tag{A-4.64}$$

Eq. (A-4.64) can be used to obtain the perturbed heat generation rates in the single-phase and two-phase regions of the heated channel. These can be further substituted into the perturbed pressure

drop in single-phase and two-phase regions of the heated channel. Finally the characteristic equation changes accordingly.

Parallel Channel Stability:

In a multi-channel system in which the channels are connected between two plenums, out-of-phase instability can occur among the channels keeping the gross flow constant. So that

$$w'_{in} = \sum_{i=1}^{N} w'_{ch,i} \tag{A-4.65}$$

The other boundary condition for analysing such a system is an equal pressure drop across the parallel channels, i.e.

$$\Delta p'_{H-SD} = \left(\Delta p'_{ch}\right)_1 = \left(\Delta p'_{ch}\right)_2 = \left(\Delta p'_{ch}\right)_N \tag{A-4.66}$$

Since $\Delta p'_{c,i} = G_i\left(w'_{ch}\right)_i$ (A-4.67)

So $w'_{in} = \Delta p'_{ch} / \sum_{i=1}^{N} G_i = 0$ (A-4.68)

Or, the characteristic equation is $\sum_{j=1}^{N}\left(\prod_{k\neq j}^{N} G_k\right) = 0$ (A-4.69)

APPENDIX–5: Nonlinear stability analysis for a single-phase NCL

The integral momentum equation applicable to one-dimensional single-phase flow in nondimensional form is (see Appendix-2 for the derivation).

$$\frac{d\omega}{d\tau} = \frac{Gr_m}{\mathrm{Re}_{ss}^3}\oint \theta\, dZ - \frac{pL_t\omega^{2-b}}{2D\,\mathrm{Re}_{ss}^b} \tag{A-5.1}$$

Similarly, the nondimensional energy equation applicable for the various segments of the loop can be written as

$$\frac{\partial\theta}{\partial\tau} + \phi\omega\frac{\partial\theta}{\partial S} = \left\{\begin{array}{c} \frac{L_t}{L_h}\ heater \quad (for\ 0 < S \le S_h) \\ 0\ \ pipes \quad (for\ S_h < S \le S_{hl}\ and\ S_c < S \le S_t) \\ -St_m\theta\ \ cooler \quad (for\ S_{hl} < S \le S_c) \end{array}\right\} \tag{A-5.2}$$

Nonlinear stability analysis is usually carried out by the direct numerical solution of the nonlinear governing equations (A-5.1) and (A-5.2) using the finite difference method. Before the calculations can commence the loop is divided into a number of small segments. A node separates two such segments (see Fig. A-5.1). Such nodes are the end nodes. Examples are N_h, N_1, etc. in Fig. A-5.1. It may be mentioned here that there are several possibilities to solve these equations such as those listed below:

1) Explicit method for both energy and momentum equations,
2) Explicit method for one of the equation along with an implicit method for the other equation or
3) Implicit method for both the equations.

The method presented here solves the energy equation explicitly and the momentum equation implicitly. The energy equation for the various segments of the loop is discretised to obtain the following equations for the temperature of the i^{th} node at the new time step (i.e. n+1) as a function of the old (i.e. n^{th}) nodal temperatures at the i^{th} and $(i-1)^{th}$ nodes.

$$\theta_i^{n+1} = \theta_i^n\left[1 - \phi\omega_n\frac{\Delta\tau}{\Delta S}\right] + \theta_{i-1}^n\left[\phi\omega_n\frac{\Delta\tau}{\Delta S}\right] + \frac{L_t\Delta\tau}{L_h} \qquad 1<N\le N_h \text{ (heater)} \tag{A-5.3}$$

$$\theta_i^{n+1} = \theta_i^n\left[1 - \phi\omega_n\frac{\Delta\tau}{\Delta S}\right] + \theta_{i-1}^n\left[\phi\omega_n\frac{\Delta\tau}{\Delta S}\right] \qquad N_h+1<N\le N_{hl} \text{ and } N_c+1<N\le N_t \tag{A-5.4}$$

$$\theta_i^{n+1} = \theta_i^n\left[1 - \phi\omega_n\frac{\Delta\tau}{\Delta S} - St_m\Delta\tau\right] + \theta_{i-1}^n\left[\phi\omega_n\frac{\Delta\tau}{\Delta S}\right] \qquad N_{hl}+1<N\le N_c \tag{A-5.5}$$

The explicit scheme has been used for the energy equation for which the stability criterion satisfying equations (A-5.3) to (A-5.5) is

$$\Delta\tau \le \frac{1}{\frac{\phi\omega_n}{\Delta S} + St_m} \tag{A-5.6}$$

To ensure stability, the calculated time step was multiplied with a number less than unity in the present calculations. The discretised momentum equation is

$$\omega_{n+1} + \frac{pL_t \Delta\tau}{2\,\mathrm{Re}_{ss}^{b}} \left|\omega_{n+1}^{1-b}\right| \omega_{n+1} = \omega_n + \frac{Gr_m \Delta\tau}{\mathrm{Re}_{ss}^{3}} \theta_I \qquad \text{(A-5.7)}$$

$$\text{Where } \theta_I = \oint \theta_i^{n+1} dZ = \int_{Z_{N1}}^{Z_{N2}} \theta_i^{n+1} dZ - \int_{Z_{N3}}^{Z_{N4}} \theta_i^{n+1} dZ \qquad \text{(A-5.8)}$$

The limits Z_{N1}, Z_{N2}, Z_{N3} and Z_{N4} correspond to the elevation at nodes N_1, N_2, N_3 and N_4 (corner nodes) respectively (see Fig. A-5.1).

Calculation Procedure

The calculations can begin after selecting a node size. The marching calculations started with node 1 and (first node in the heater) equation (A-5.3) was used to calculate the nodal temperatures for $1<N\leq N_h$. From $N_h+1<N\leq N_{hl}$ equation (A-5.4) was used. Similarly, equation (A-5.5) was used for $N_{hl}+1<N\leq N_c$. For the cold leg equation (A-5.4) was used for $N_c+1<N\leq N_t$. Once all the nodal temperatures are calculated the temperature integral, θ_I, is numerically evaluated using the Simpson's rule. Then ω_{n+1} is obtained by solving Eq. (A-5.7) numerically using the Newton-Raphson or the bisection method.

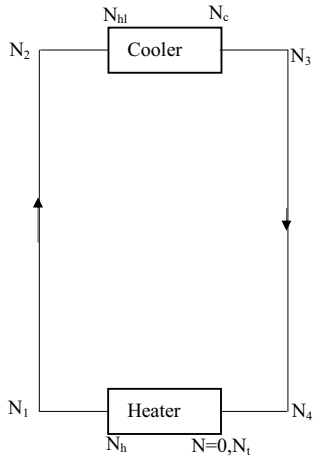

FIG. A-5.1. Nodalization for clockwise flow

The adequacy of the nonlinear formulation can be checked by comparing with the analytical steady state equations. Also, the stability threshold predicted by the code can be compared with the corresponding threshold obtained by the linear method. For this comparison, the initial conditions corresponded to the steady state value for the orientation considered.